THE GEOLOGICAL SOCIETY OF AMERICA®

Temporally constant slip rate along the Ganzi fault, NW Xianshuihe fault system, eastern Tibet

Marie-Luce Chevalier[1,†], Philippe Hervé Leloup[2,†], Anne Replumaz[3,†], Jiawei Pan[1,†], Marianne Métois[2,†], and Haibing Li[1,†]

[1]*Key Laboratory of Continental Dynamics, Institute of Geology, Chinese Academy of Geological Sciences, 26 Baiwanzhuang Road, Beijing 100037, People's Republic of China*

[2]*Laboratoire de Géologie de Lyon, CNRS UMR 5570, Université de Lyon 1, 69622 Villeurbanne, France*

[3]*Institut des Sciences de la Terre (ISTerre), Université Grenoble Alpes, 38058 Grenoble, France*

ABSTRACT

The left-lateral strike-slip Xianshuihe fault system, located in eastern Tibet, is one of the most tectonically active intracontinental fault systems in China, if not in the world, along which more than 20 M >6.5 earthquakes have occurred since A.D. 1700, including the 2010 Mw 6.9 Yushu earthquake. It is therefore essential to precisely determine its slip rate, which remains poorly constrained at all time scales, in order to evaluate regional earthquake hazard. Here, we focus on the NW segment of the Xianshuihe fault system, the Ganzi fault. We studied three sites where the active Ganzi fault cuts and left-laterally offsets moraine crests and fan edges. We constrained left-lateral offsets using light detection and ranging (LiDAR) and kinematic global positioning system (GPS) methods, and we used cosmogenic dating to determine the abandonment age of the offset surfaces. We found that the slip rate remains constant along the entire Ganzi fault (~300 km) at 6–8 mm/yr at the late Quaternary time scale, consistent with geodetic (interferometric synthetic aperture radar [InSAR] and GPS) as well as geologic slip rates (4.9–7.5 mm/yr since ca. 12.6 Ma). This implies that the Manigango segment of the Ganzi fault could potentially produce a M 7.6 earthquake in the near future. While the Xianshuihe fault system propagated from west to east, the fact that the Ganzi fault's long-term slip rate is similar to that of the Xianshuihe fault to the SE suggests that the onset of the Xianshuihe fault system at ca. 13 Ma marked a major transition in tectonic regime in SE Tibet.

INTRODUCTION

The left-lateral strike-slip Xianshuihe fault system, located in eastern Tibet, is considered to be one of the most tectonically active intracontinental fault systems on Earth (e.g., Molnar and Deng, 1984; Allen et al., 1991; Wen, 2000; Wen et al., 2008). Almost the entire fault system has ruptured since A.D. 1700, with nine earthquakes of Ms >7 and 16 earthquakes of Ms >6. Along the central segment, the Xianshuihe fault, three earthquakes of Ms >7.3 have occurred since 1923 (Allen et al., 1991; Wen, 2000), producing surface rupture up to 110 km long and coseismic offsets up to 5.5 m. The NW segment, consisting of the Yushu/Batang and Ganzi faults, seems less active, even though several large-magnitude earthquakes have occurred since the late 1800s (Table 1), including the 2010 Mw 6.9 Yushu earthquake (star #3 in Fig. 1A), which produced 70 km of surface rupture along the Yushu fault, with coseismic offsets of 1–2 m (e.g., Li et al., 2012; Zhang, 2013).

Following the Yushu earthquake, the Yushu fault has been extensively studied using interferometric synthetic aperture radar (InSAR) methods (e.g., Li et al., 2011; Liu et al., 2011; Tobita et al., 2011; G. Zhang et al., 2016) and field investigations (e.g., Lin et al., 2011; Li et al., 2012), giving a broad estimation of the present-day slip rate of 2–10 mm/yr. Late Quaternary horizontal slip rates along the Ganzi fault (Table 2) also show large uncertainties, between 3 and 14 mm/yr (e.g., Zhou et al., 1996; Wen et al., 2003; Xu et al., 2003; Shi et al., 2016; colored dots in Fig. 1D) using offset-age reconstructions

TABLE 1. HISTORICAL EARTHQUAKES ALONG THE GANZI FAULT

Date	Magnitude	Surface rupture length (km)	Horizontal offset (m)	References
Batang-Dengke				
1896	7.3	70	~3–5	Zhou et al. (1997, 2014); Wen et al. (2003); Cheng et al. (2011)
1100 ± 70		?		Zhou et al. (2014)
1550 ± 110		?		Zhou et al. (2014)
Dengke-Manigango				
1320 ± 65	8	170?	5–9	Zhou et al. (1997); Wen et al. (2003); Cheng et al. (2011)
Manigango-Ganzi				
1854	7.3	170	<9	Zhou et al. (1997); Cheng et al. (2011); Wen et al. (2003)
1866	7.7	65	3.6–6.3	Wen et al. (2003); Cheng et al. (2011)
1982	6	10		Roth (1989)
Zhuwo fault				
1811	6.7	15		IGCEA and HGFU (1990)
1919	6.5	20		Roth (1989)
1967	6.8	18	0.68	Zhou et al. (1983); Papadimitriou et al. (2004); Cheng et al. (2011)

†mlchevalier@hotmail.com; herve.leloup@univ-lyon1.fr; anne.replumaz@ujf-grenoble.fr; jiawei-pan@foxmail.com; marianne.metois@univ-lyon1.fr; lihaibing06@163.com.

GSA Bulletin; https://doi.org/10.1130/B31691.1; 10 figures; 3 tables; Data Repository item 2017269.

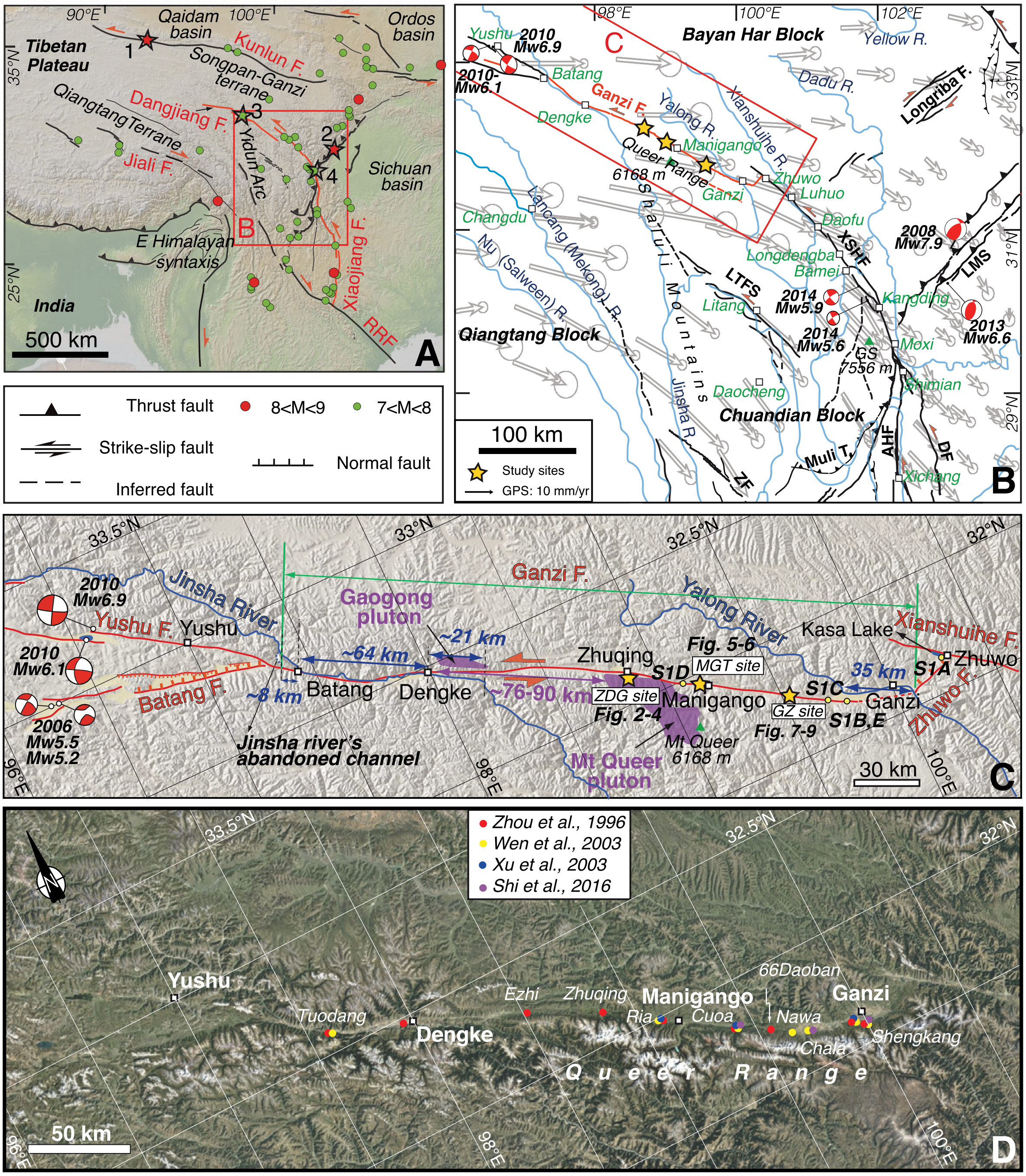

Figure 1. The Xianshuihe fault system in the frame of the India-Asia collision zone. (A) Tectonic map of the eastern Himalayan syntaxis region with digital elevation model (DEM) in the background. Xianshuihe fault system is shown in red. RRF—Red River fault. Stars indicate locations of major earthquakes along the Bayan Har block (Songpan Ganzi terrane): 1—2001 Ms 8.1 Kokoxili earthquake, 2—2008 Ms 8.0 Wenchuan earthquake, 3—2010 Mw 6.9 Yushu earthquake, 4—2013 Ms 7.0 Lushan earthquake. (B) SE Tibetan Plateau with horizontal global positioning system (GPS) velocities relative to stable Eurasia (Liang et al., 2013), focal mechanisms of instrumental earthquakes with Mw >5 (Centroid Moment Tensor [CMT] catalogue 1976–2016): 2008 Wenchuan, 2010 Yushu, 2013 Lushan, 2014 Kangding, as well as main peaks, cities, and faults. LTFS—Litang fault system, XSHF—Xianshuihe fault, LMS—Longmen Shan, GS—Gongga Shan, ZF—Zhongdian fault, AHF—Anninghe fault, DF—Daliangshan fault. (C) DEM of the Yushu/Batang faults and Ganzi fault region, with active faults in red and main rivers in blue. Yellow stars show locations of the three study sites (Zhuqing [ZDG], Manigango [MGT], and Ganzi [GZ]), with corresponding figure numbers. Yellow dots locate pictures found in the supplementary information S1 (see text footnote 1). Purple areas represent the plutons discussed in the text. (D) Google Earth image of the Yushu/Batang faults and Ganzi fault region, on which the high peaks (covered by glaciers) of the Queer Range are very clear just south of the fault, in contrast to the more subdued reliefs north of the fault. Colored dots refer to the four studies where late Quaternary slip rates were determined.

TABLE 2. SLIP RATE SUMMARY ALONG THE GANZI FAULT

Slip rate (mm/yr)	Reference	Method	Ref. in Fig. 10
14.4 ± 1.5	Gan et al. (2007)	GPS (strain rate analysis)	1
10–11 ± 0.3	Loveless and Meade (2011)	GPS (block model)	2
6.6 ± 1.5	Wang et al. (2013)	GPS (profiles)	3
11 ± 1	Thatcher (2007)	GPS (block model)	4
10 ± 2	Shen et al. (2005)	GPS Yunnan + Sichuan	5
12	Meade (2007)	GPS (block model)	6
12.6–14.7	Wang et al. (2017)	GPS (block model)	7
6.4	Liu et al. (2011)	InSAR	8
Batang-Dengke			
7.2 ± 1.2	Zhou et al. (1996)	Thermoluminescence dating	9
11.3 ± 1.8*	Wen et al. (2003)	Thermoluminescence dating	/
9.8 ± 0.9	Zhou et al. (2014)	Paleoseismology	10
Dengke-Manigango			
7 ± 0.7	Zhou et al. (1996)	Thermoluminescence dating	11
<10 ± 0.4	Shi et al. (2016)	^{14}C, paleoseismology	12
12.8 ± 1.7*	Wen et al. (2003)	^{14}C	/
13.4 ± 2*	Xu et al. (2003)	Thermoluminescence dating	/
4.3–11.2	**This study, Ria site**	Reinterpretation of Xu et al. (2003) using MGT age	Ria
3–8.3	**This study, MGT site**	^{10}Be	MGT
7 (+1.1/–1.0)	**This study, ZDG site**	^{10}Be	ZDG
Manigango-Ganzi			
8.5 (+0.8/–0.7)	**This study, GZ site**	^{10}Be	GZ
13.0 ± 1.7	Wang et al. (2008)	GPS (fault model)	13
3.4 ± 0.3	Zhou et al. (1996)	Thermoluminescence dating	14
11.5 ± 2.4*	Wen et al. (2003)	Thermoluminescence dating	/
8 ± 1	Shi et al. (2016)	Reinterpretation of Wen et al. (2003)	15
2.6–8.3	Shi et al. (2016)	^{14}C, paleoseismology	16
Queer Shan pluton			
6.6 (+0.8/–0.7)	Wang et al. (2009)	76–90 km in 12.6 ± 1 m.y.	17
Jinsha River			
6.2 ± 1.3		64 to 93 km in 12.6 ± 1 m.y.	18

Note: GPS—global positioning system; InSAR—interferometric synthetic aperture radar; MGT—Manigango; ZDG—Zhuqing; GZ—Ganzi.
*Rates obtained using the lower terrace reconstruction, and therefore overestimated. See text for details.

(with ^{14}C, optically stimulated luminescence [OSL], or thermoluminescence [TL] dating), and 9–15 mm/yr using paleoseismology (Zhou et al., 2014). Farther south, the Xianshuihe fault has been investigated using morphotectonic methods, giving a higher Holocene to late Quaternary average slip rate of 10–20 mm/yr (e.g., Allen et al., 1991; Y. Zhang et al., 2016). On the long-term time scale, poorly constrained slip rates of 3.5 to 30 mm/yr along the Xianshuihe fault system have been suggested by matching geological offsets of ~60–100 km (e.g., Wang et al., 1998; Wang and Burchfiel, 2000; Zhang, 2013; Yan and Lin, 2015) with initiation ages of ca. 2–17 Ma (e.g., Roger et al., 1995; King et al., 1997; Wang et al., 1998; Wang and Burchfiel, 2000; Yan and Lin, 2015). Such variability between short-term (global positioning system [GPS], InSAR) and some longer-term (tectonic-geomorphology, geochronology) slip rates is common (e.g., Hanks and Thatcher, 2006; Thatcher, 2007), partly due to measurements over different periods of the earthquake cycle, related to crust and mantle rheology below the seismogenic zone (Savage and Prescott, 1978; Segall, 2002; Perfettini and Avouac, 2004). Late Quaternary rates span multiple earthquake cycles, so they minimize interseismic strain accumulation or postseismic relaxation, while geodetic measurements span only a few years and therefore do not necessarily represent what is happening over the long term (thousands to millions of years). Geodetic rates are prone to vary during the earthquake cycle due to slow-slip events or temporal variations of interseismic coupling, and they may not be stable over several seismic cycles (e.g., Rogers and Dragert, 2003). Consequently, geodetic techniques may underestimate or overestimate slip rates if they are measured only over one limited interseismic period, or if the fault is late in its earthquake cycle (when an earthquake is overdue). This can have dramatic consequences if the importance of a fault in accommodating deformation is mistakenly assessed. Therefore, precise constraints on fault slip rates at the late Quaternary time scale are essential to assess seismic hazards, especially in this highly active zone of eastern Tibet, where one can assess how deformation due to the India-Asia collision is accommodated.

Our study fills the geographic gap between the Yushu fault and the Xianshuihe fault, as well as the time gap between geodetic and geological slip-rate data by doing a morphotectonic study of the Ganzi fault using ^{10}Be cosmogenic radionuclides, which has not yet been done. In this paper, we present three study sites where the Ganzi fault cuts and left-laterally (as well as vertically at places) offsets late Quaternary geomorphic markers such as moraines and alluvial fans. We used a combination of high-resolution satellite image observations and field surveys (including terrestrial light detection and ranging [LiDAR] and kinematic GPS), as well as ^{10}Be cosmogenic dating of the offset geomorphic markers, to determine late Quaternary slip rates. We compare the slip rates obtained at various time scales and assess the seismic hazard along the Ganzi fault.

GEOLOGICAL SETTING

The NW-striking Xianshuihe fault system has a relatively simple geometry with distinct stepovers and bends that control the rupture terminations and allow segments to be defined (e.g., Klinger, 2010; Zielke et al., 2015). The Xianshuihe fault system consists of the Yushu (from west of Yushu to the city of Batang) and Ganzi (from Batang to Ganzi Cities) faults in the NW, the Xianshuihe fault (from approximately the town of Zhuwo to the town of Moxi) in the middle, and the Anninghe-Zemuhe-Xiaojiang faults in the SE (Fig. 1B; e.g., Allen et al., 1991). The entire fault system is ~1400 km long and a few hundred meters wide in most places, except in the SE part, where the Xianshuihe fault system splays in several active, right-stepping branches that strike approximately N-S until reaching the Red River fault (Fig. 1A). The Xianshuihe fault system acts as a bounding fault that limits the northern extent of the clockwise rotation of material with respect to Eurasia, around the eastern Himalayan syntaxis, as evidenced by GPS data (e.g., Zhang et al., 2004; Shen et al., 2005).

The far NW Xianshuihe fault system is made up of two converging faults, the Yushu fault in the north, which ruptured in 2010, and the Batang fault in the south, which has a normal component opening wide sedimentary basins just west of Batang (Fig. 1C). East of Batang, the Jinsha River follows the Ganzi fault for ~60 km between Batang and Dengke (Fig. 1C), making it hard to clearly follow the fault trace in this deep valley (Fig. 1D). Once the Jinsha River leaves the fault near Dengke to veer to the SE, the Ganzi fault becomes clearer in the topography as it follows the northern flank of the Queer Range. The dogleg shape of the Jinsha River has been interpreted to reflect a 60–90 km offset by the fault (Wang et al., 1998; Wang and Burchfiel, 2000; Fig. 1C). The NW-trending Queer Range, which culminates at 6168 m elevation, belongs to the Shaluli Mountains, which constitute the NW end of the larger-scale Hengduan Mountains of eastern Tibet (Fig. 1B). Interestingly, the prominent Queer Range is only present SW of the Ganzi fault, while NE of the fault, the reliefs are more subdued (Fig. 1D). This possibly reflects recent uplift of the SW compartment of the fault. East of Dengke, the fault trace is very clear, with numerous pull-apart basins and sag ponds (Figs. S1D and S1E[1]), shutter ridges (Figs. S1B and S1E [see footnote 1]), and offset geomorphic markers attesting to its left-lateral component. Where the Ganzi fault enters the Ganzi Basin, it is harder to follow, partly due to human activities, even though the presence of hot springs attests to the importance of fault activity (Fig. S1E [see footnote 1]). There, the Yalong River appears to be offset by ~35 km by the Ganzi fault (Wang et al., 1998; Fig. 1C). The three sites we investigated in detail are located along the eastern half of the Ganzi fault, just north of the Queer Range, where the fault cuts numerous moraines (sites Zhuqing [ZDG] and Ganzi [GZ]) and several river terraces or fans (site Manigango [MGT]). A left en-echelon step-over just east of the town of Ganzi, between the Ganzi and Xianshuihe faults, forms an ~25-km-wide pull-apart basin (Fig. 1C). There, the NE-striking Zhuwo normal fault (dipping to the NW at 50°–65°; Papadimitriou et al., 2004) marks the SE side of the basin.

METHODOLOGY

In order to map active fault strands and geomorphic surfaces, and to precisely measure offsets, we used a combination of field investigation and high-resolution satellite images, such as Google Earth or Bing images, as well as high-resolution topographic data from a Riegl VZ1000 terrestrial LiDAR scanner (angular resolution of 0.02° for raw data, set to <0.5 m horizontally and <0.2 m vertically between two data points after filtering the data) and from a kinematic GPS (Trimble R8). The ^{10}Be cosmogenic radionuclide dating technique (e.g., Gosse and Phillips, 2001) allowed us to precisely constrain the surface emplacement exposure ages of the study sites: 10 and 12 samples were collected from the top few centimeters of large granite boulders present on the ZDG and GZ moraine crests, respectively, and one depth profile from a refreshed terrace riser at the MGT fan site. The offset of the fan edges or moraine crests was taken between the piercing points on both sides of the fault. Then, matching the age of the surfaces with their offset yielded median slip rates at the 1σ level (calculated using Zechar and Frankel, 2009) at the late Quaternary time scale.

Several factors, however, may influence the ^{10}Be concentration in the samples we collected. Most processes, such as erosion, weathering, snow cover, and rolling, yield young apparent ages (e.g., Putkonen and Swanson, 2003; Applegate et al., 2010; Chevalier et al., 2011; Heyman et al., 2011), whereas inherited cosmogenic radionuclides (due to prior exposure) will overestimate the ages (e.g., Heyman et al., 2011). However, it appears that only 3% of the boulders ("outliers") may have been exposed prior to glacial erosion, transport, and deposition (Putkonen and Swanson, 2003; Heyman et al., 2011), especially since glacial boulders have been pulled off from the glacial valley, crushed, and eroded before sitting on a moraine's crest. Those outliers have ages that are much older than the rest of the population and can be discarded (e.g., Benedetti and Van der Woerd, 2014). In addition, while a moraine is overall a relatively stable feature over the long term, a moraine surface is generally unstable after its emplacement, with large boulders being gradually exhumed to the surface as erosion washes the smaller material away, thus representing various stages of exhumation as the surface lowers. Therefore, in the absence of clear outliers, it is most appropriate to choose the oldest age of the sample population to represent the emplacement age of the moraines (e.g., Hallet and Putkonen, 1994; Putkonen and Swanson, 2003; Briner et al., 2005; Applegate et al., 2010; Chevalier et al., 2011; Heyman et al., 2011).

In order to constrain the age of alluvial surfaces or glacial outwash when no suitable samples are present on their surface (such as at the MGT fan site), we used the amalgamated clasts approach (e.g., Anderson et al., 1996; Repka et al., 1997; Hancock et al., 1999; Matmon et al., 2009) by collecting samples from a depth profile. This approach assumes that the inherited component in each clast is small enough so that it can be averaged through the amalgamation, i.e., that the sediments have been deposited rapidly enough to be considered as a single stratigraphic unit (which appears to be the case for the MGT fan site; see following), especially for large catchments (Hetzel et al., 2002) such as the MGT fan site.

SITES DESCRIPTION AND RESULTS

Zhuqing (ZDG) Moraines

The impressive Zhuqing (ZDG) moraine complex, out of the Yingpu valley, is located ~120 km NW of Ganzi (~32.112°N, 98.851°E; Fig. 1C). The moraines are located at elevations of ~4000–4200 m and originate from a 5816-m-high peak of the NW Queer Range, where a large ice cap is still present, and from which several glaciers flow northward to the Zhuqing Basin (Fig. 2B). The ZDG moraine complex is made of >14 different crests, from only a few meters high to ~200 m high (Ou et al., 2014). An ~10-m-high scarp is visible across the valley, nicely showing the fault's trace (Figs. 2B and 2C). No glacial lake remains in the valley, but large swamps are still present downstream from the fault (Fig. 2). The main ZDG lateral moraines are steep, ~4-km-long, 2-km-wide, 200-m-high moraines (Fig. 3A), and their crests are relatively subrounded and covered with small bushes and occasional trees, with numerous large (up to ~10 m diameter) boulders. Two recessive inner latero-frontal moraines (younger) are visible along the inner flanks of the main ZDG moraines (Figs. 2B, 2C, and 3) and have been dated at 16.2 ± 1.4 ka and 12.2 ± 1.1 ka by Ou et al. (2014) using OSL dating (Fig. 2A). While the upstream inner moraines are preserved and uplifted by the fault, their downstream equivalents have been downdipped by the fault and are now covered by the swamps (Fig. 2C).

We collected 10 samples on the western main crest (Fig. 2A; Table 3), from the top of large embedded granite boulders (Fig. S2 [see footnote 1]). Seven samples were collected upstream from the fault (ZDG1–ZDG7), and three were collected downstream (ZDG8–ZDG10). The ages range from 14 ± 1 ka to 23 ± 2 ka (Fig. 4; Table 3), with no difference between the samples collected upstream and downstream from the fault, attesting that it is a single moraine. As explained above, we chose the oldest age of 23 ± 2 ka to best represent the moraine emplacement age, considering that no anomalously old sample is present here. That age is consistent (i.e., older) with that of the inner moraines. Surveying the site using a terrestrial LiDAR as well as a kinematic GPS along the western crest allowed us to precisely measure its left-lateral offset, which is 160 ± 20 m (Fig. 3). The offset of the eastern crest is smaller (~80 m) due to the left-lateral sense of motion along the fault and the postglacial erosion of the eastern lateral

[1]GSA Data Repository item 2017269, field photos of several geomorphic features along the active Ganzi fault (location in Fig. 1C) (Fig. S1), photos of individual boulders we collected at Zhuqing (ZDG) and Ganzi (GZ) moraines (Fig. S2 and S4, respectively), details on the parameters used in the software of Hidy et al. (2010) (Fig. S3), and GPS profiles across the Ganzi fault (Fig. S5), is available at http://www.geosociety.org/datarepository/2017 or by request to editing@geosociety.org.

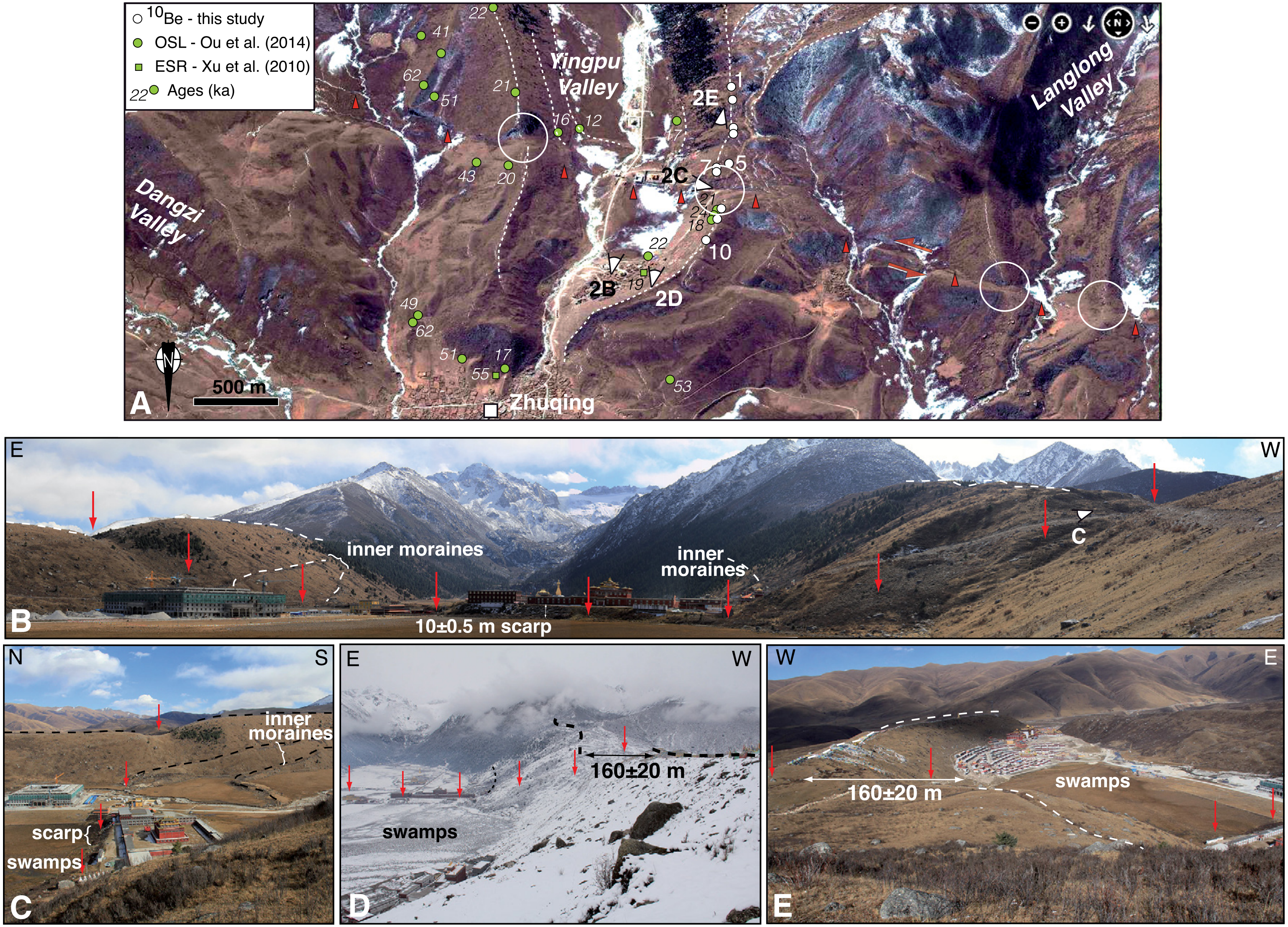

Figure 2. Field photos of the Zhuqing (ZDG) moraine site. (A) Bing satellite image of the ZDG site. Ages (in ka) from other studies are shown next to sample locations. Circles highlight offsets. (B) Panoramic photo looking upstream toward the present-day glacier. The fault, highlighted by red arrows, offsets the eastern and western moraine crests. Note the fault scarp and the inner moraines on the flanks of the valley. (C) View of the eastern moraine offset, the inner moraines, and the fault scarp. (D) Offset of the western moraine crest. (E) View looking downstream, showing the terminal moraines and downstream western crest. Note the presence of large swamps. OSL—optically stimulated luminescence; ESR—Electron Spin Resonance.

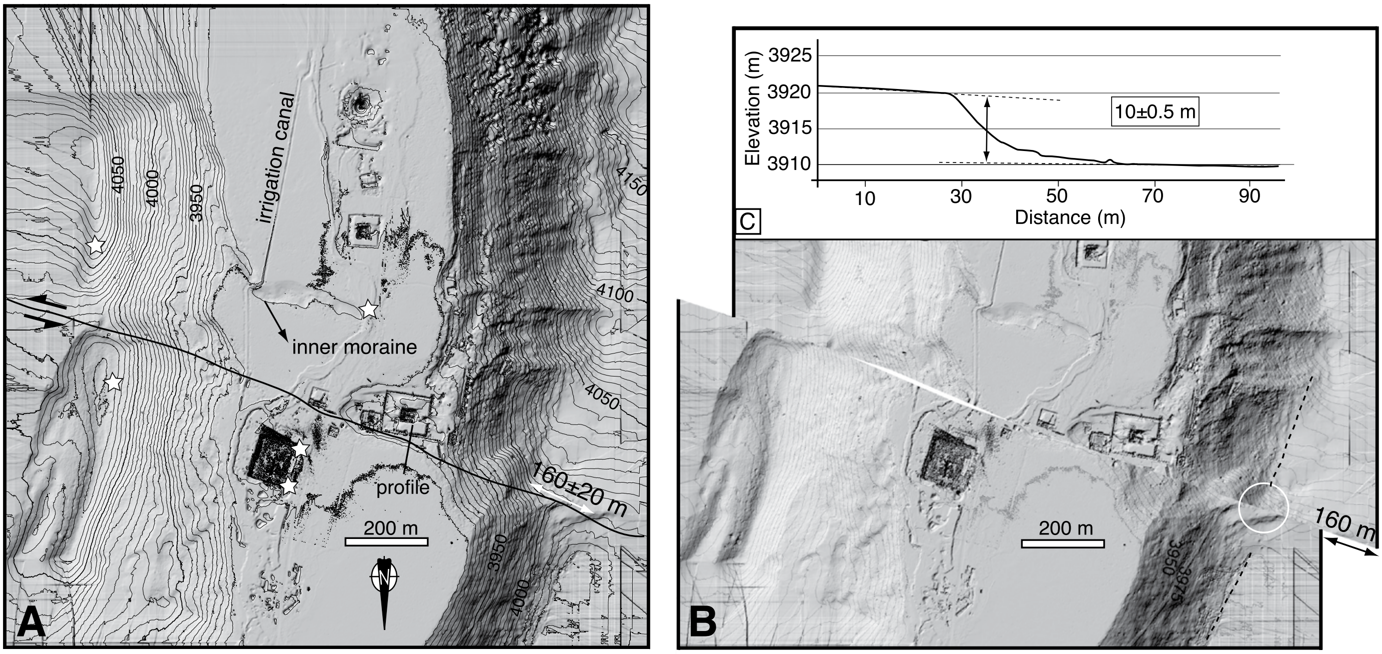

Figure 3. Digital elevation model of Zhuqing (ZDG) moraines site (~32.112°N, 98.851°E). (A) High-resolution digital elevation model determined from terrestrial light detection and ranging (LiDAR) survey (contours in m). Locations of LiDAR bases are represented by white stars. Note that elevations are approximate (LiDAR data give accurate relative, not absolute, elevation) and slightly differ from those obtained from the topographic contours. (B) 160 ± 20 m backslip of LiDAR data realigns the crests highlighted in black. (C) Topographic profile across the fault scarp (location in A).

moraine in the downstream area. The fault scarp is 10 ± 0.5 m high on the valley floor (Figs. 2B, 2C, 3A, and 3C). Matching the 160 ± 20 m offset with the 23 ± 2 ka age of the western moraine crest yields a late Quaternary horizontal slip rate of 7 +1.1/–1.0 mm/yr. A vertical throw rate of >0.4 mm/yr for the southern (upstream) area was estimated from the offset of the valley floor (10 m in 23 ± 2 k.y.), or >0.6 mm/yr taking the 16.2 ka age of Ou et al. (2014) for the upper inner moraine (Fig. 2A).

Manigango (MGT) Fan

The Manigango (MGT) fan site is located ~30 km SE of the ZDG moraines and ~8 km NW of the town of Manigango (~31.964°N, 99.135°E; Fig. 1C), at ~4000 m elevation. The fan and terraces were emplaced at the apex of an ~7-km-long moraine (Fig. 5D) coming from the central Queer Range, where very few present-day glaciers remain. The Ganzi fault cuts through the fan and terraces and left-laterally offsets their risers (Figs. 5 and 6). The fan and terraces upstream from the fault are significantly higher (up to 12 ± 1 m) than those downstream from the fault, attesting to a locally important vertical component of motion (Figs. 6B and 6C).

The MGT fan surfaces are flat (4° slope) and covered by short grass and small bushes at places. The active main stream (river 1) has entrenched 15 ± 1 m (measured by LiDAR) into the fan, and only two levels of terraces (T3 and T2) are present around river 1. The terraces are devoid of large boulders, and smaller rocks have been disturbed by human interaction due to seasonal settlement and by small animals. We consequently refreshed the upstream, western T3/T2 riser (Fig. 5C) and collected numerous cobbles (~5 cm diameter) from the same depth, every 20 cm at eight different depths, and processed them as eight single samples (see Methodology section). However, because the top and bottom levels did not yield enough quartz, we only have data for six different depths, from 50 to 150 cm below the fan's surface (Fig. 6D; Table 3). In order to model the ^{10}Be concentration obtained at different depths to determine a surface age, we used the software of Hidy et al. (2010), which yielded a surface age for the T3 fan surface of 19 ± 2.3 ka (Fig. 6D; Fig. S3 [see footnote 1]). This age suggests that the MGT fan was emplaced soon after the Last Glacial Maximum (LGM, ca. 20 ka; e.g., Clark et al., 2009), following glacier retreat and possible breach of the frontal moraine.

After the MGT fan was emplaced, its edges could start to be offset by the fault. The eastern edge of the fan appears to be offset by a maximum of 130 ± 20 m, since the current stream that follows the downstream edge of the fan may have eroded it (Fig. 5B). Subsequently, the fan surface itself (T3) started to be entrenched by streams such as rivers 1 and 2 (Fig. 5B) and form terraces such as T2. Eventually, the terrace risers started to be offset. Detailed site surveying using terrestrial LiDAR and kinematic GPS yielded horizontal offsets of the main abandoned gullies and terrace risers ranging from ~20 to ~75 m (Figs. 5B and 6B). Note that the 75 ± 16 m offset of the T3/T2 riser (taken as an average between the riser's top-to-top and bottom-to-bottom offsets) is a minimum due to the constant erosion of its upstream riser by river 1, while the downstream riser is preserved (Fig. 5B). The vertical offsets we measured are 9 ± 1 m for T3 west of river 1 (profile P2), and 12 ± 1 m for T3 east of river 1 (profile P3; Fig. 6C).

Matching the MGT fan (T3) surface age with the fan's maximum offset (130 ± 20 m) yields a maximum slip rate of 6.8 +1.5/–1.2 mm/yr, while matching the largest minimum offset of T3/T2 (75 ± 16 m) with the age of T3 yields a minimum slip rate of 3.9 +1.0/–0.9 mm/yr. Matching the largest vertical offset of T3 (12 ± 1 m) with the age of T3 yields a vertical throw rate of 0.6 ± 0.1 mm/yr. Therefore, the horizontal slip rate at the MGT fan site ranges from 3 to 8.3 mm/yr. The highest horizontal slip rate determined at the MGT site is close to the slip rate

TABLE 3. ANALYTICAL RESULTS OF ^{10}BE GEOCHRONOLOGY AND SURFACE EXPOSURE AGES ALONG THE GANZI FAULT

Sample name	Lat (°N)	Long (°E)	Elev. (m)	Depth (cm)	Quartz (g)	Be carrier (mg)	^{10}Be–^{9}Be ($\times 10^{-15}$)	^{10}Be ($\times 10^{6}$ atoms/gram)	Desilets ages§ (yr)	Dunai ages§ (yr)	Lifton ages§ (yr)	LS indep ages§ (yr)	**LS dep ages§ (yr)**
Zhuqing (ZDG)													
Upstream from fault													
ZDG-1†	32.109997	98.85129	4144	–	29.3288	0.3458048	944 ± 30	0.741 ± 0.023	13,533 ± 1659	14,097 ± 1721	13,090 ± 1360	14,146 ± 1312	**13,982 ± 1263**
ZDG-2†	32.110398	98.851279	4138	–	21.9617	0.3083264	844 ± 29	0.789 ± 0.027	14,386 ± 1776	14,914 ± 1834	13,909 ± 1459	15,112 ± 1420	**14,878 ± 1362**
ZDG-3*	32.112183	98.851023	4111	–	27.5069	0.30553955	1250 ± 18	0.924 ± 0.013	16,783 ± 2006	17,221 ± 2050	16,193 ± 1624	17,952 ± 1592	**17,431 ± 1501**
ZDG-4*	32.112113	98.851143	4110	–	30.2901	0.4085192	1161 ± 17	1.042 ± 0.016	18,672 ± 2245	19,059 ± 2281	17,962 ± 1815	20,231 ± 1812	**19,480 ± 1695**
ZDG-5*	32.114641	98.851186	4060	–	27.4762	0.3907093	1144 ± 17	1.083 ± 0.016	19,824 ± 2382	20,173 ± 2414	19,056 ± 1923	21,553 ± 1928	**20,663 ± 1795**
ZDG-6*	32.115006	98.851970	4049	–	25.9056	0.39167	1174 ± 17	1.182 ± 0.018	21,593 ± 2591	21,872 ± 2613	20,740 ± 2089	23,696 ± 2114	**22,531 ± 1952**
ZDG-7*	32.114519	98.852399	4050	–	27.4163	0.3927046	966 ± 16	0.92 ± 0.015	17,238 ± 2079	17,662 ± 2121	16,625 ± 1687	18,434 ± 1661	**17,863 ± 1564**
Downstream from fault													
ZDG-8†	32.117665	98.852038	4038	–	22.3229	0.3014656	1106 ± 37	0.994 ± 0.032	18,600 ± 2292	18,988 ± 2330	17,901 ± 1872	20,053 ± 1876	**19,321 ± 1761**
ZDG-9*	32.118361	98.852347	4037	–	27.9462	0.398321	1178 ± 18	1.118 ± 0.017	20,732 ± 2490	21,050 ± 2517	19,916 ± 2008	22,618 ± 2021	**21,602 ± 1875**
ZDG-10†	32.119341	98.85278	4036	–	23.5206	0.2927616	915 ± 29	0.758 ± 0.024	14,610 ± 1793	15,126 ± 1848	14,131 ± 1470	15,280 ± 1420	**15,032 ± 1360**
Manigango (MGT)													
MGT-2*	31.964071	99.135594	3992	150	27.7061	0.36244255	224 ± 7	0.192 ± 0.007	–	–	–	–	–
MGT-3*	31.964071	99.135594	3992	130	28.5678	0.35372235	352 ± 9	0.287 ± 0.008	–	–	–	–	–
MGT-4*	31.964071	99.135594	3992	110	25.8842	0.387236	271 ± 8	0.267 ± 0.009	–	–	–	–	–
MGT-5*	31.964071	99.135594	3992	90	28.0030	0.38779025	413 ± 10	0.378 ± 0.01	–	–	–	–	–
MGT-6*	31.964071	99.135594	3992	70	26.7842	0.3879011	456 ± 10	0.437 ± 0.01	–	–	–	–	–
MGT-7*	31.964071	99.135594	3992	50	32.9849	0.38771635	753 ± 13	0.588 ± 0.011	–	–	–	–	–
Ganzi (GZ)													
Upstream from fault													
GZ-1*	31.728473	99.5791	4037	–	27.6338	0.38623835	2944 ± 30	2.745 ± 0.028	44,472 ± 5345	43,661 ± 5223	42,257 ± 4250	56,132 ± 5007	**47,905 ± 4137**
GZ-2*	31.728449	99.579118	4037	–	31.4787	0.3860536	2012 ± 25	1.645 ± 0.02	29,066 ± 3479	29,010 ± 3457	27,848 ± 2791	33,427 ± 2965	**30,602 ± 2633**
GZ-3*	31.728569	99.577947	4046	–	27.0613	0.3863492	1264 ± 19	1.202 ± 0.018	21,927 ± 2630	22,205 ± 2652	21,049 ± 2119	24,125 ± 2151	**22,856 ± 1979**
GZ-4*	31.728672	99.577378	4050	–	29.7080	0.3861275	5969 ± 47	5.18 ± 0.041	85,673 ± 10,419	83,390 ± 10,088	80,459 ± 8172	106,812 ± 9655	**92,631 ± 8088**
GZ-5*	31.728657	99.576364	4059	–	27.4303	0.3808067	476 ± 11	0.437 ± 0.011	8514 ± 1029	9161 ± 1103	8351 ± 852	8703 ± 789	**8590 ± 758**
GZ-6*	31.728642	99.575935	4064	–	28.2208	0.3641053	757 ± 14	0.649 ± 0.012	12,433 ± 1493	13,028 ± 1558	12,044 ± 1216	12,881 ± 1153	**12,750 ± 1109**
GZ-7*	31.728826	99.573827	4086	–	26.8417	0.3908571	3640 ± 34	3.537 ± 0.033	57,037 ± 6873	55,618 ± 6669	53,091 ± 5346	70,834 ± 6331	**61,868 ± 5351**
Downstream from fault													
GZ-8*	31.731137	99.580608	3998	–	28.0882	0.39104185	3711 ± 34	3.448 ± 0.031	58,660 ± 7073	57,361 ± 6883	54,762 ± 5519	72,207 ± 6458	**63,033 ± 5455**
GZ-10B†	31.731971	99.581753	3981	–	20.8881	0.2883584	2883 ± 52	2.649 ± 0.047	44,286 ± 5362	43,502 ± 5243	42,106 ± 4279	55,634 ± 5029	**47,481 ± 4159**
GZ-11†	31.731592	99.581215	3992	–	15.2355	0.3004416	3893 ± 80	5.111 ± 0.105	87,523 ± 10,790	85,154 ± 10,444	82,218 ± 8512	108,600 ± 10,057	**94,061 ± 8425**
GZ-12†	31.731267	99.580712	3999	–	12.9872	0.2930688	2729 ± 58	4.100 ± 0.086	69,367 ± 8505	67,801 ± 8272	65,543 ± 6753	86,184 ± 7930	**74,770 ± 6662**
GZ-13†	31.731492	99.581215	3993	–	27.8388	0.3176448	2724 ± 49	2.069 ± 0.037	36,091 ± 4358	35,705 ± 4291	34,537 ± 3501	43,015 ± 3871	**37,951 ± 3313**

Note: All samples are granite; shielding factor is 0.98; sample density is 2.7 g/cm^3; thickness is ~5 cm. No erosion rate was applied. Ages were calculated with the CRONUS 2.2 (with constants 2.2.1) calculator. Age references: Desilets et al. (2006); Dunai (2000, 2001); Lifton et al. (2005). LS dep (indep)—Lal (1991)/Stone (2000) time-dependent (independent) production rate models.

*Samples were processed and measured at GNS Science in New Zealand. Standard used at GNS is "01-5-4" with ^{10}Be isotope ratios = 2.85×10^{-12}, equivalent to 07KNSTD.

†Samples were processed at the Institute of Crustal Dynamics in Beijing, and ^{10}Be/^{9}Be ratios were measured at ASTER (Accélérateur pour les Sciences de la Terre, Environnement, Risques; CEREGE [Centre Européen de recherche et d'enseignement des Géosciences de l'Environnement]). Standard used at ASTER is NIST SRM4325 (=NIST_27900) with ^{10}Be isotope ratios = 2.79×10^{-11}, equivalent to 07KNSTD.

§External uncertainties (analytical and production rate; Balco et al., 2008) are reported at the 1σ confidence level.

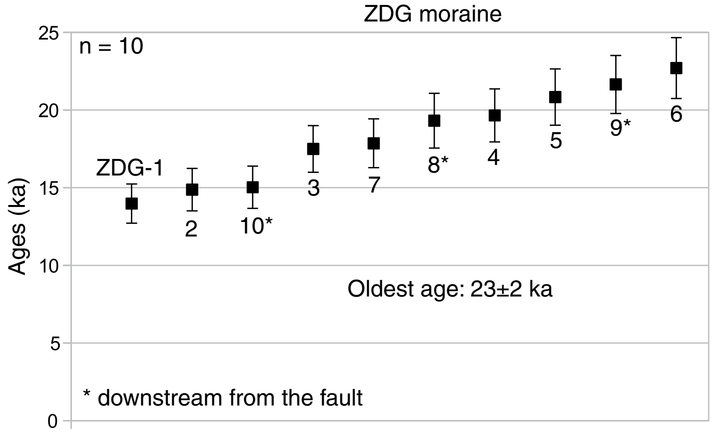

Figure 4. Ages of Zhuqing (ZDG) moraines, showing ^{10}Be cosmogenic surface exposure ages (using the time-dependent model of Lal, 1991/ Stone, 2000 ["LS dep" column, bold in Table 3]) with 1σ uncertainty.

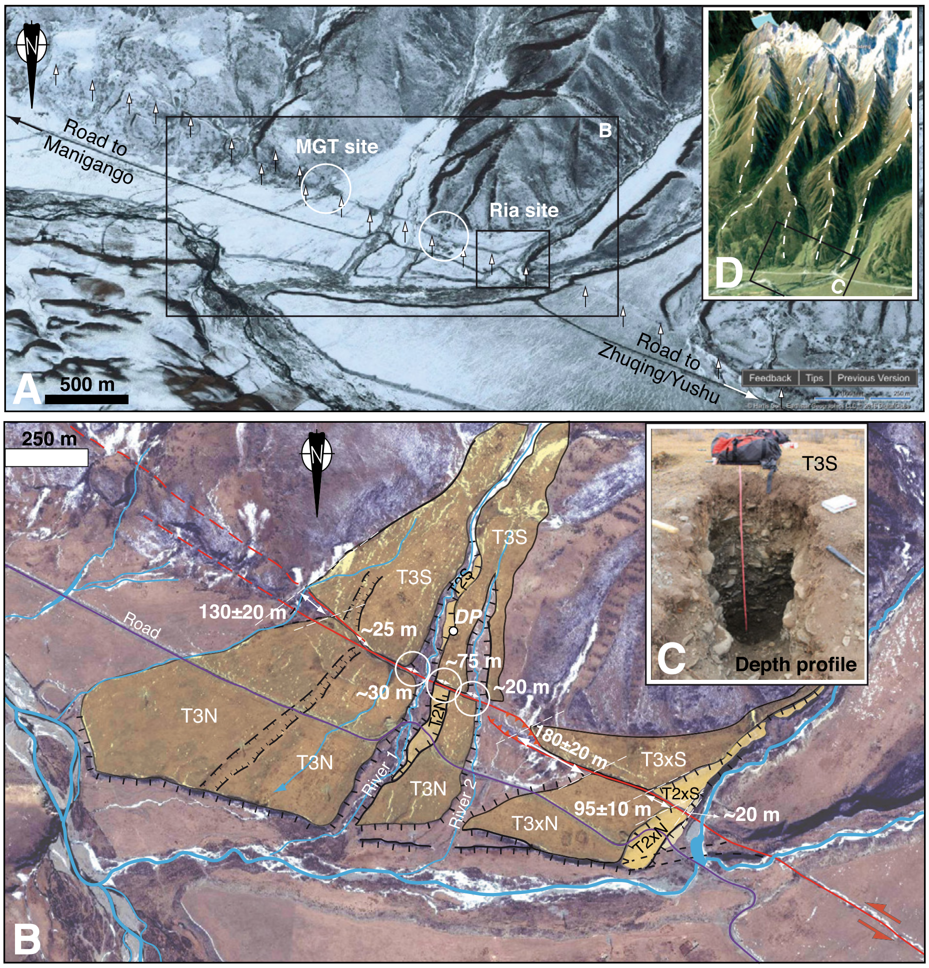

Figure 5. Manigango (MGT) and Ria sites (~31.964°N, 99.135°E). (A) Area near the MGT and Ria fan sites on Bing images and (B) close-up. Fault is highlighted by white arrows in A. Depth profile (DP) location is shown in B. (C) Photo of depth profile from T3/T2 riser at the MGT site. (D) Google Earth image of the entire MGT valley as well as neighboring valleys, where moraine crests are highlighted with white dashed lines (vertical exaggeration 3×).

determined at the ZDG site (7 +1.1/–1.0 mm/yr) at the same ~20 k.y. time scale.

Ganzi (GZ) Moraines

The Ganzi fault, trending ~N120° at that location, bounds the SE Queer Range, and one can follow its trace all the way to Ganzi (Fig. 1C). It cuts and left-laterally offsets several moraines, including the ones that extend the farthest to the north, where our Ganzi (GZ) moraines stand, ~40 km NW of Ganzi (~31.731°N, 99.581°E) at elevations of ~4000 m (Fig. 1C). The fault also vertically offsets late Quaternary deposits with the north (downstream) side up (Figs. 7 and 8).

The moraines were emplaced by glaciers flowing down from the SE Queer Range, where present-day glaciers abound (Fig. 1D). Numerous large U-shaped glacial valleys and moraines extend north of the range for ~2 km before veering to the NE (1 in Fig. 7C). Upstream from that turn, moraines with rough topography and large boulders diverge out of the main valley toward the NW ("1" in Fig. 7C; pink tones in Fig. 7A). The main GZ moraines (smoother topography, crests highlighted by white dashed lines in Fig. 7A) extend farther and cross the fault. They are covered by grass and small bushes (Fig. S4 [see footnote 1]), and medium-sized granodiorite boulders (up to 2.5 m large and up to 1.2 m above the surface) with big quartz grains lie on their crests (Fig. S4 [see footnote 1]). Swamps are present between the eastern and western GZ crests as well as along the fault (Fig. 8A).

We collected 12 samples from the top of the largest boulders (Fig. S4 [see footnote 1]) that were present on the surface of the western crests, seven upstream from the fault (GZ1–GZ7) and five downstream (GZ8–GZ13; Fig. 8A). GZ sample ages are widespread and range from 8.6 ± 0.8 ka to 94 ± 8 ka (Fig. 9; Table 3). This large age spread may be explained by the fact that the crests are smooth, and the boulders are medium sized (Fig. S4 [see footnote 1]), compared to, for example, those present at ZDG. Indeed, it has been shown that large boulders yield a better representative age of a moraine's emplacement than smaller ones (Heyman et al., 2016). While one could imagine that the upstream and downstream crests do not belong to the same moraine, the fact that their ages are indistinguishable most likely indicates that they are part of the same moraine complex. As explained already, we take the oldest age of the surface to represent the emplacement age of the moraine, 94 ± 8 ka, which, taking into account the error bars, could correspond to marine oxygen isotope stage (MIS) 5b or 5c (Fig. 9). As far as we know, no other MIS 5 moraines have been found in eastern Tibet.

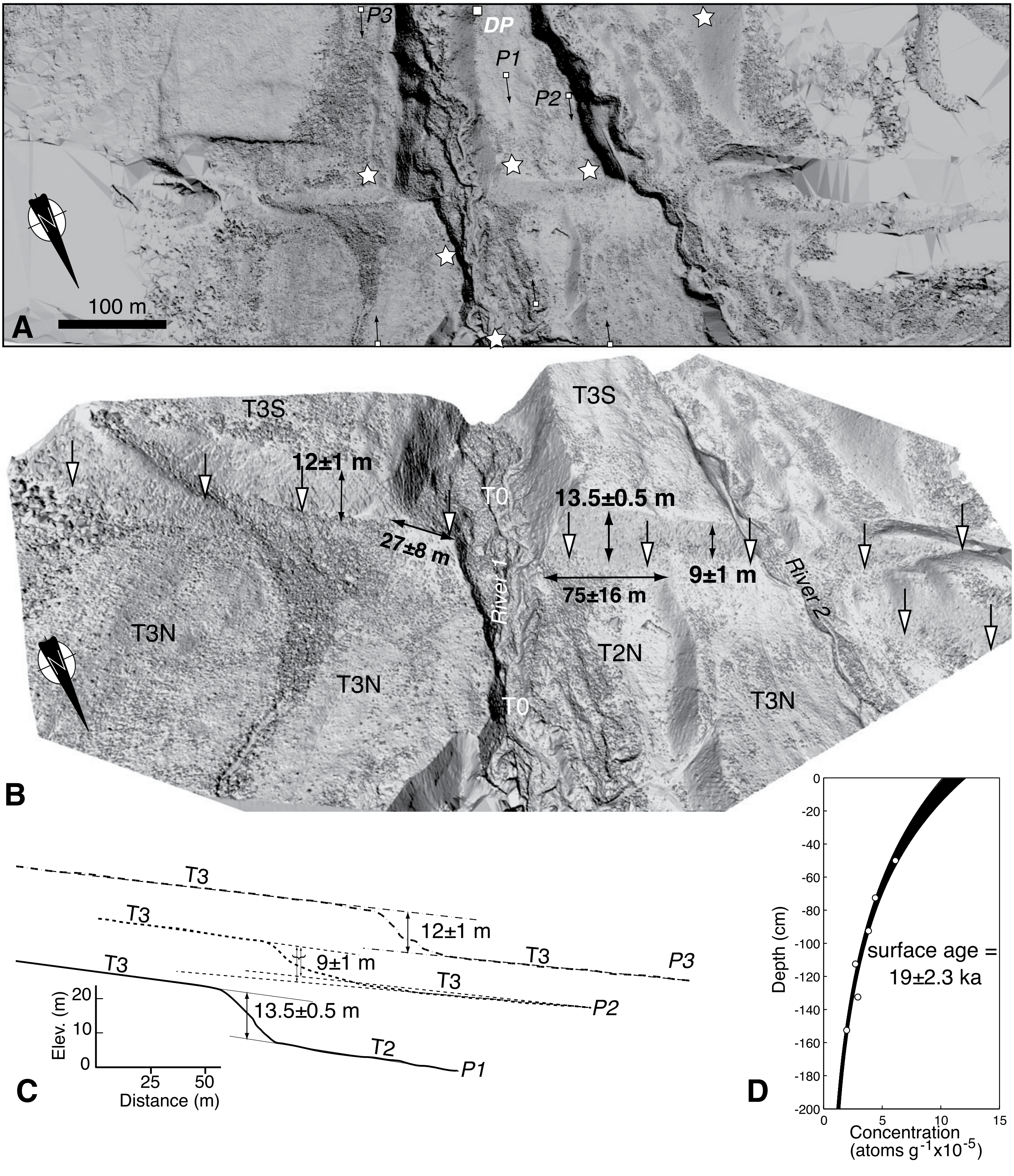

Figure 6. Digital elevation model (DEM) of Manigango (MGT) site (~31.964°N, 99.135°E). (A) Terrestrial light detection and ranging (LiDAR) DEM with locations of profiles perpendicular to the fault. White stars show locations of LiDAR bases. (B) General three-dimensional LiDAR DEM of the central part of the MGT fan site where vertical and minimum horizontal offsets are visible. Fault trace is highlighted by white arrows. (C) LiDAR profiles perpendicular to the fault, showing the vertical offsets of T3 and T3/T2. (D) MGT ^{10}Be surface age (T3) obtained by modeling the depth profile samples using the software of Hidy et al. (2010). See details in Figure S3 (see text footnote 1).

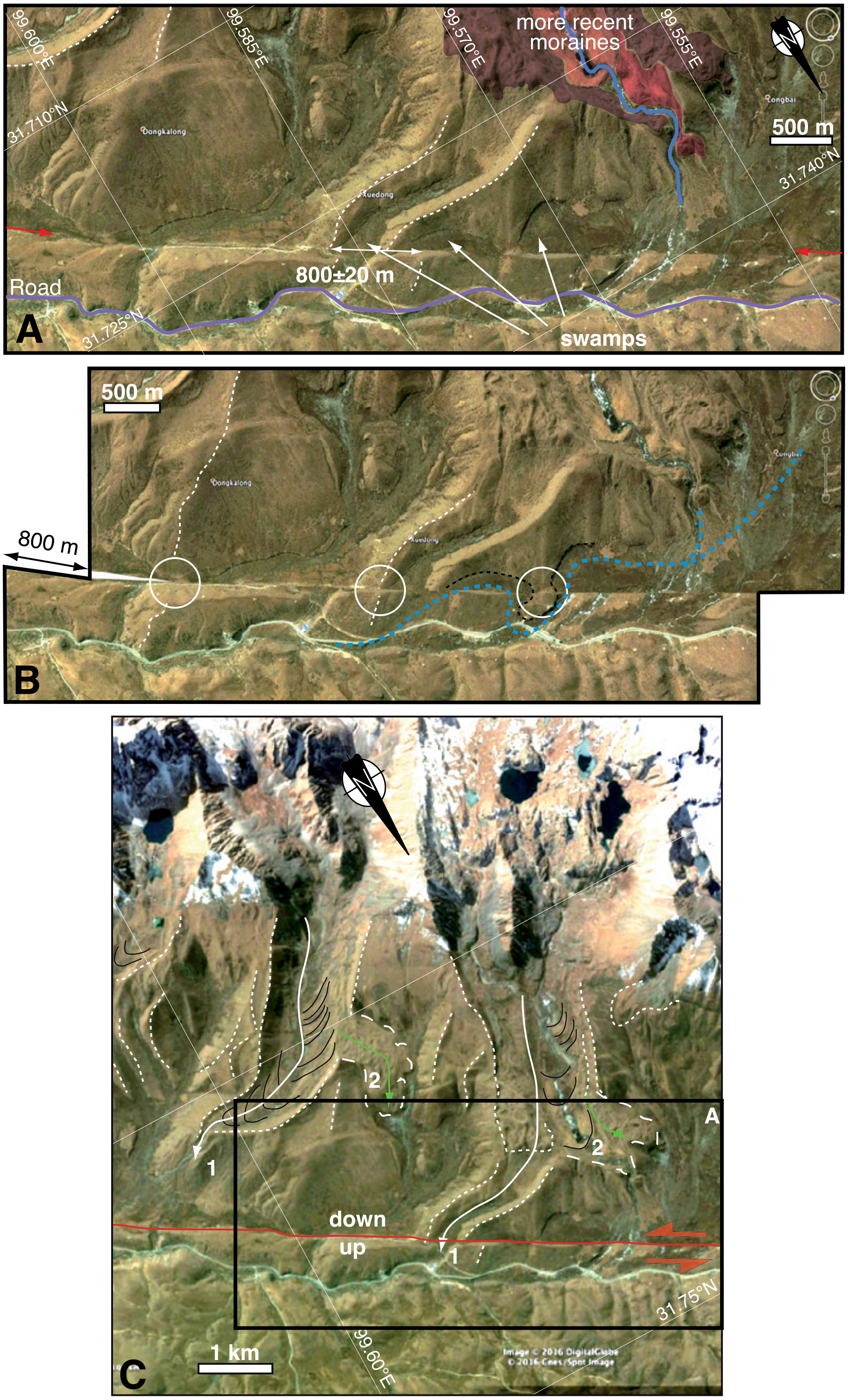

Figure 7. Ganzi (GZ) moraine site area (~31.731°N-99.581°E). (A) Google Earth image corresponding to the black frame in C, with its interpretation. (B) Backslipping of satellite image showing the 800 ± 20 m offset of the eastern moraine crest as well as of two other features. Blue dashed line represents possible course of former river. (C) Google Earth image of the area around GZ site. Ganzi fault is shown in red, and moraine crests are shown as white dashed lines. "1" refers to moraines that extend north of the range for ~2 km before veering to the NE. Upstream from that turn, "2" refers to moraines with rough topography and large boulders, which diverge out of the main valley towards the NW.

We surveyed the GZ site using LiDAR and kinematic GPS, which yielded a left-lateral offset of 800 ± 20 m by realigning (1) the eastern upstream crest with the western downstream crest; (2) a small hill and promontory that may have been the inner part of a river meander prior to being offset (blue dashed line in Fig. 7B); as well as (3) another moraine crest to the east (dashed lines in Figs. 7B and 8B). Matching the 800 ± 20 m offset with the 94 ± 8 ka age yields a left-lateral slip rate of 8.5 +0.8/–0.7 mm/yr, similar to what we determined at the ZDG and MGT sites.

DISCUSSION

Ganzi Fault Slip Rate at Various Time Scales

Late Quaternary Slip Rates

ZDG site. We determined the emplacement age of the ZDG moraines at 23 ± 2 ka using ^{10}Be dating, which roughly corresponds to the Last Glacial Maximum (LGM, ca. 20 ka). Other studies sampled the same crests with different techniques and determined similar ages (Fig. 2A) of: 22.2 ± 1.7 ka (four samples between 19.7 and 22.2 ka using OSL; Ou et al., 2014), 24.3 ± 2 ka (three samples between 18.4 and 24.3 ka using OSL; Xu et al., 2010; but recalculated by Ou et al., 2014), 18.5 ± 1.9 ka (one sample using ESR [electron spin resonance]; Xu et al., 2010), and 24.7 ± 2 ka (one sample using TL, Dangzi moraine nearby [Fig. 2A]; Lehmkuhl, 1998). Our results are in agreement with other studies from the Hengduan Mountains, which determined that LGM moraines are regionally widespread (e.g., Strasky et al., 2009; Xu and Zhou, 2009; Zhang et al., 2012). Therefore, we are confident about the ZDG moraines being LGM in age, and, consequently, we are confident about the slip rate 7 +1.1/–1.0 mm/yr we obtained using the offset at the ZDG site.

MGT site. While moraines are very large and steady features with clear crests, fan surfaces are more transient. Fan edges and terrace risers may easily be eroded after fan emplacement as the river and newly formed gullies entrench the fan surface. Minimum and maximum offset values are often given, corresponding to different erosion phases not always easily datable.

At the MGT site (Fig. 5), we determined the fan age (T3) at 19 ± 2.3 ka using ^{10}Be dating. Such large fan deposition has been interpreted as a consequence of post-LGM massive melting (e.g., Clark et al., 2009). We measured the maximum offset of the eastern edge of T3 at 130 ± 20 m and the minimum offset of the T3/T2 riser at 75 ± 16 m, leading to a horizontal slip rate ranging between 3 and 8.3 mm/yr.

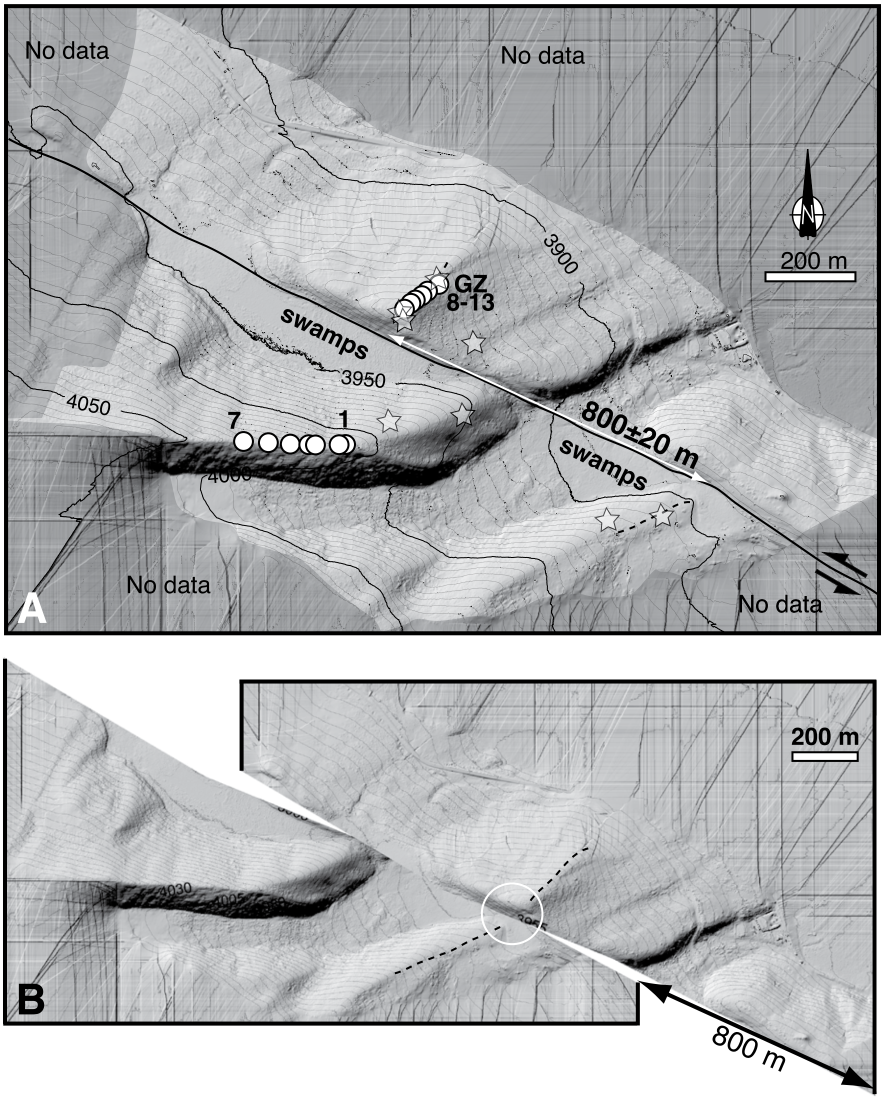

Figure 8. Digital elevation model of the Ganzi (GZ) moraines site (~31.731°N-99.581°E). (A) High-resolution digital elevation model (DEM) determined from terrestrial light detection and ranging (LiDAR) survey (contours in m). Locations of LiDAR bases are represented by white stars. Note that elevations are approximate (LiDAR data give accurate relative, not absolute, elevation) and slightly differ from those obtained from the topographic contours. (B) 800 ± 20 m backslip of LiDAR data realigns the crests highlighted in black. GZ samples are shown as white circles.

Five hundred meters west of the MGT site, the Ria site has a very similar geometry with a fan surface (T3x) similar to T3 at MGT, also entrenched by a stream, and a lower terrace (T2x) similar to T2 at MGT (Figs. 5A and 5B). The eastern edge of T3x is offset by a maximum of 180 ± 20 m, and the T3x/T2x riser is offset by 95 ± 10 m. T2x was dated at 7.4 ± 0.6 ka (one ^{14}C age; Wen et al., 2003) and 6.62 ± 0.52 ka (one TL age; Xu et al., 2003), and T3x was dated at 11.12 ± 0.93 ka (one TL age; Xu et al., 2003), surprisingly approximately twice as young as our T3 surface at MGT.

A maximum slip rate of 14.3 +2.0/–1.8 mm/yr had been suggested by matching the T3x/T2x riser offset with the lower terrace T2x age (Xu et al., 2003; Wen et al., 2003). However, because a riser may constantly be refreshed by the active river until the lower terrace is abandoned, taking the upper terrace age (T3x) yields a maximum age for the offset and thus a minimum slip rate (e.g., Cowgill, 2007): >8.5 +1.2/–1.1 mm/yr (95 m in 11 k.y.). However, due to the fact that Xu et al. (2003) had only one sample for each terrace, compared to our six depth profile samples at the MGT site, we consider that our T3 age at MGT is more robust, and we apply it to the offsets at the Ria site. This yields horizontal slip rates ranging between 5 +0.9/–0.7 mm/yr (180 ± 20 m in 19 ± 2.3 k.y.) and 9.5 +1.7/–1.4 mm/yr (95 ± 10 m in 19 ± 2.3 k.y.), i.e., between 4.3 and 11.2 mm/yr, in agreement with what we obtained at the MGT site. Nevertheless, additional dating will be necessary to confirm the ages of the terraces at the Ria site.

GZ site. The GZ site shows a left-lateral offset of 800 ± 20 m of moraine crests dated at 94 ± 8 ka (MIS 5c), i.e., older than the LGM moraines at the ZDG site, which yields a left-lateral slip rate of 8.5 +0.8/–0.7 mm/yr. This is the first time that a slip rate along the Xianshuihe fault system has been determined for such a long time interval, as previous studies documented only LGM or younger offset geomorphic features. This rate is very similar to what we determined at the LGM time scale at the ZDG site (7 +1.1/–1.0 mm/yr), and it is also within the range of slip rates we determined at the MGT/Ria sites (3–11.2 mm/yr) farther to the NW.

Geological Slip Rates

The Ganzi fault is continuous without major change in fault direction or fault bifurcation at the scale of ~300 km (Fig. 1B). The total left-lateral geological offset along the fault can be estimated in two different ways. First, the geologic formations show an offset of ~80 km. South of the fault, the eastern part of the Qiangtang terrane corresponds to the approximately N-S–trending Permian–Triassic Yidun volcanic arc, which contains Triassic (ca. 245 to ca. 216 Ma) and Cretaceous (ca. 105–95 Ma) granitoids (Reid et al., 2007). That arc is bent, cut, and offset by the Xianshuihe fault system near Manigango. Among the granitoids south of the fault, the Queer Shan granite is cut by the fault and matches the Gaogong granite on the other side of the fault, indicating a 76–90 km left-lateral offset (Fig. 1C; Wang and Burchfiel, 2000; Wang et al., 2009). Apatite fission-track (AFT) ages from the pluton are older than 17 Ma, indicating that most of its exhumation occurred prior to that time, while AFT ages from within the fault zone are all younger than 12.6 ± 1 Ma, suggesting that fault initiation occurred at that time (Wang et al., 2009). Considering a 76–90 km offset in 12.6 ± 1 m.y. yields a left-lateral slip rate of 6.6 +0.8/–0.7 mm/yr. Second, the Jinsha River has a dogleg shape near Batang, suggesting ~100 km of left-lateral offset (Fig. 1C; Wang and Burchfiel, 2000). In more detail, the river follows the fault for 64 km, but abandoned valleys north and south of the fault can accrue offset by 8 and 21 km, respectively, suggesting a total offset of 64–93 km (Fig. 1C). That corresponds to a rate of 6.2 ± 1.3 mm/yr,

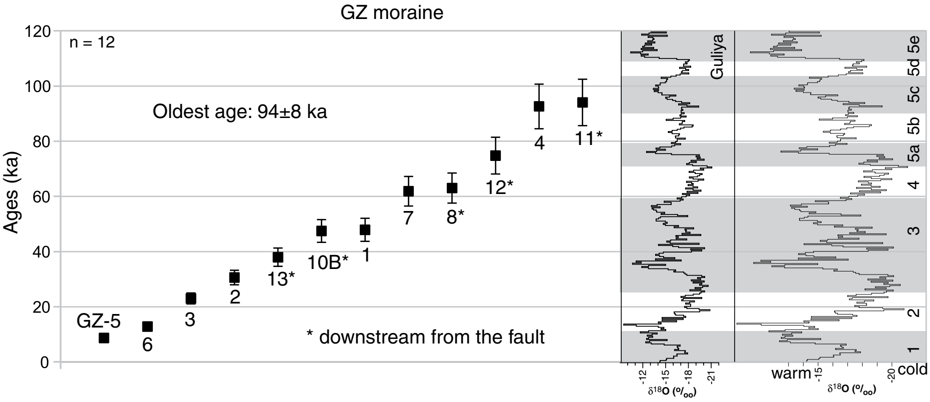

Figure 9. Ages of Ganzi (GZ) moraines, showing ^{10}Be cosmogenic surface exposure ages (using the time-dependent model of Lal, 1991/Stone, 2000 ["LS dep" column, bold in Table 3]) with 1σ uncertainty. Figure also shows the Specmap climatic proxy curve of Thompson et al. (1997) from the Guliya ice cap in western Tibet, and that of Imbrie et al. (1984; right panel), with gray-shaded sectors showing the marine oxygen isotope stages (MIS).

considering that the river entrenchment is older than the fault's initiation at 12.6 ± 1 Ma.

Geodetic Slip Rates

At a much shorter time scale (a few years), rates along the Ganzi fault can be calculated using GPS data. The GPS network is improving rapidly, so we take into account only the most recent results, but it is still sparse, and high uncertainties remain. Wang et al. (2013) recently calculated a strike-slip rate of 6.6 ± 1.5 mm/yr along the Ganzi and Yushu/Batang faults, with a low shortening rate of 1.7 ± 1.6 mm/yr. This result was obtained by defining a Chuandian block fixed reference frame using few core stations south of the Ganzi fault. In order to better constrain that rate from stations located close to the fault trace, we analyzed two recent GPS data sets across the Ganzi fault near Manigango (Fig. S5 [see footnote 1]). The two data sets are sparse and yield a large range of possible left-lateral slip rates: 3.3 ± 3.6–5.4 ± 2.6 mm/yr for that of Liang et al. (2013) and 1.6 ± 0.9–4.4 ± 0.9 mm/yr for that of Zhao et al. (2015), and no significant extension (Fig. S5 [see footnote 1]).

To reduce the uncertainty due to the sparse GPS network, synthetic three-dimensional elastic block models have been built at the scale of all of Tibet to estimate the rate that is most compatible with all available GPS data. Using 17 blocks, Meade (2007) determined a left-lateral slip rate of 12 mm/yr along the Ganzi fault, while using 24 blocks, Loveless and Meade (2011) inferred a similar rate of ~10–11 ± 0.3 mm/yr. Assuming 11 blocks, Thatcher (2007) suggested an overall horizontal rate (both along and across strike) of 11 ± 1 mm/yr. Considering a global rigid rotation of Tibet rather than defining block boundaries, Gan et al. (2007) proposed an even faster rate: 14.4 mm/yr. Recently, Wang et al. (2017) estimated a slip rate on the Xianshuihe fault between 12.6 and 14.7 mm/yr from geodetic data only or including geologic observations, respectively.

Slip Rate Comparison at Various Time Scales

At the late Quaternary time scale, the slip rate of the MGT site ranges between 3 and 8.3 mm/yr; at the Ria site, it ranges between 4.3 and 11.2 mm/yr; at the ZDG site, it is 7 +1.1/–1.0 mm/yr; and at GZ, it is 8.5 +0.8/–0.7 mm/yr (Fig. 10; Table 2). Considering that the ZDG site is the most robust (clear offset and similar ages), and that the rates at the GZ and MGT/Ria sites are compatible with that at ZDG, we suggest a late Quaternary slip rate along the Ganzi fault of 6–8 mm/yr (gray shaded area in Fig. 10). This rate encompasses late Quaternary studies from Zhou et al. (1996) and Shi et al. (2016). At the longer-term time scale, matching the pluton offset (76–90 km) and the Jinsha River offset (64–93 km) with the fault's initiation age (12.6 ± 1 Ma) yields a geological slip rate of 4.9–7.5 mm/yr (Fig. 10; Table 2), which falls into the 6–8 mm/yr late Quaternary slip rate range we suggest.

At the geodetic time scale, the GPS data of Wang et al. (2013) and Liang et al. (2013) and the InSAR data of Liu et al. (2011) are compatible with values we obtained at longer time scales (6–8 mm/yr). However, the Zhao et al. (2015) GPS data set yields a slightly slower rate (Fig. 10; Table 2), which may be due to reference frame differences or regional impact of the postseismic rebound of the nearby 2008 Wenchuan earthquake. All other published GPS slip rates (open symbols in Fig. 10) appear to be significantly faster than the 6–8 mm/yr slip rate we suggest for all time scales. This may show the limitations of the global approach, as numerous active faults are present within the Chuandian block, such as the en-echelon Litang fault system (Fig. 1B), along which some segments are purely normal and have a slip rate of ~0.6 mm/yr since 6 Ma, opening up large basins (Zhang et al., 2015; Chevalier et al., 2016). Therefore, based on the relatively good agreement between slip rates measured on short-term (GPS), late Quaternary (ca. 90–20 ka), and geologic (ca. 13 Ma) time scales, we suggest that the slip

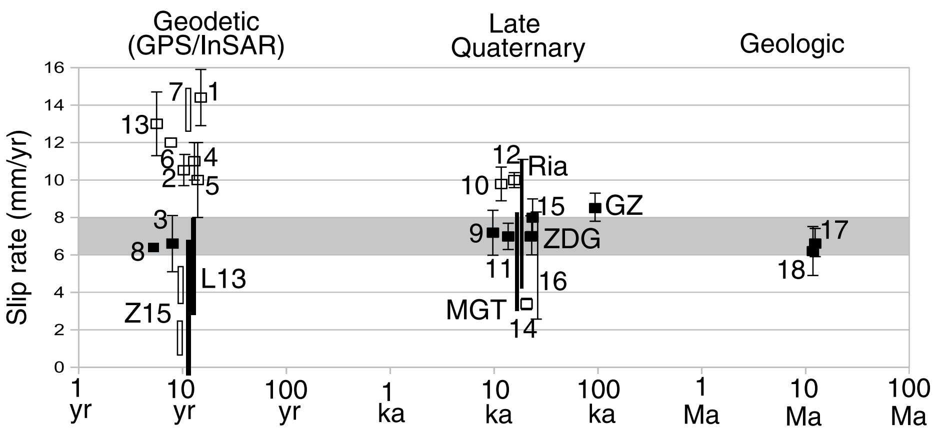

Figure 10. Horizontal slip rates along the Ganzi fault at the three study sites (Zhuqing [ZDG], Manigango [MGT], and Ganzi [GZ]) at various time scales. See Table 2 for references to numbers. L13—Liang et al. (2013), Z15—Zhao et al. (2015). Open symbols represent rates that are not in agreement with the 6–8 mm/yr (gray shaded area) slip rate we suggest for all time scales. GPS—global positioning system; InSAR—interferometric synthetic aperture radar.

rate along the Ganzi fault has remained constant at 6–8 mm/yr.

Late Quaternary Slip Rates along the Xianshuihe Fault System

Near Batang, at the NW extremity of the Ganzi fault, the Xianshuihe fault system splits into two branches: the Batang and Yushu faults (Fig. 1B). The Batang fault has been described as a left-lateral reverse fault by Huang et al. (2015a, 2015b), who suggested late Quaternary slip rates of 2–4 mm/yr using offset geomorphic landforms. However, according to our mapping and field observations, the Batang fault opens wide sedimentary basins just west of Batang, attesting to its normal component. Such a normal component is expected on a N100°-trending fault connected to a left-lateral fault trending N130° such as the Ganzi fault. In addition, we did not find any systematic horizontal offsets, even if a few small gullies may appear offset as suggested by Huang et al. (2015a, 2015b). However, these authors documented clear vertical offsets of ~6 m of a fan surface dated at ca. 24 ka, equivalent to our T3 surfaces, giving a rough estimate of the vertical rate of ~0.25 mm/yr. To the north, the Yushu fault appears to have purely strike-slip motion, as indicated by focal mechanisms of the 2010 Mw 6.9 Yushu earthquake (Fig. 1C), but no morphotectonic determination of the Yushu fault slip rate is available to date.

The Holocene left-lateral slip rate along the Xianshuihe fault SE of the Ganzi fault has been inferred at 15 ± 5 mm/yr using three terrace riser offsets of ~140–200 m (near Luhuo and Longdengba, Fig. 1B) inferred to be postglacial, with a poorly constrained age between 7.5 ka (one sample using ^{14}C) and 20 ka (LGM; Allen et al., 1991). Nevertheless, considering that these postglacial terraces have the same age as our MGT fan (19 ± 2.3 ka), the slip rate for the Xianshuihe fault would become 6.5–12 mm/yr. Therefore, the 6–8 mm/yr rate we determined along the Ganzi fault would appear on the lower end of that along the Xianshuihe fault, which may suggest a southeastward increase in horizontal slip rates along the Xianshuihe fault system, even though additional quantitative data are warranted to constrain the rates along the other segments of the Xianshuihe fault system.

Geodynamic Significance of the Xianshuihe Fault System

The Xianshuihe fault system is 1400 km long and veers around the eastern Himalayan syntaxis (Fig. 1A). In this study, we constrain its left-lateral slip rate at ~7 mm/yr along its Ganzi segment at the late Quaternary time scale, as well as since ca. 12.6 Ma. This rate is similar to the long-term left-lateral slip rate proposed for the Xianshuihe segment of the Xianshuihe fault system that has accrued an offset of 62 km since ca. 9 Ma (Zhang et al., 2017). It thus appears that the different segments of the Xianshuihe fault system have been activated at different times, with the Xianshuihe fault system propagating toward the east, despite the fact that the fault slip rate seems to be similar along all segments at all time scales. We do not discuss in this paper the timing of initiation of the eastern part of the fault system (Anninghe-Zemuhe-Xiaojiang faults; Fig. 1B) because precise constraints on age and slip rate there are still lacking, even if it has been proposed that these segments are more recent (Wang et al., 1998). Such geometry, constant slip rate, and propagation from west to east of a fault system are expected when a rigid body (India) indents a plastic media having a free boundary with shape similar to that of the South China–Sundaland continental lithosphere (Tapponnier and Molnar, 1976). We thus suggest that in SE Tibet, a major tectonic reorganization occurred between ca. 17 and 15 Ma, corresponding to the end of the southeastward extrusion of Sundaland (e.g., Leloup et al., 2001), and ca. 12.6 Ma, corresponding to the initiation of the Xianshuihe fault system. That latter initiation time marks the onset of the present-day tectonic regime. This tectonic regime is characterized by a strong rotation of the maximum horizontal compression from N-S at the front of the indenter in the eastern Himalaya to approximately E-W at the western boundary of the indented continent along the Sagaing fault in Burma (e.g., Tapponnier and Molnar, 1976). In such context, it is not necessary to invoke lower-crustal channel flow to explain the geometry of the active faults and the associated deformation pattern around the eastern Himalayan syntaxis.

Earthquake Hazard Along the NW Xianshuihe Fault System

The 2010 Yushu earthquake proved that the Yushu fault is active. Along the Ganzi fault, numerous large earthquakes (up to M 7.7) have occurred since A.D. 1800, except near Manigango where the last large earthquake was 700 yr ago (believed to be M 8, and therefore having longer recurrence interval; Table 1). Interestingly, only the Yushu/Batang faults have a different geometry than the others, with several faults rather than a single continuous fault. The fact that the large Yushu earthquake (Mw 6.9) occurred along such a discontinuous and geometrically complicated segment may suggest that an even larger earthquake is more likely to occur along the Ganzi fault farther to the SE. Indeed, taking our 6–8 mm/yr slip rate, the slip deficit near Manigango reaches ~5 m (since 700 yr), which, considering an ~150 km rupture length (Manigango segment), yields a potential earthquake of magnitude of 7.6 at present ($M = 5.08 + 1.16 \times \log$[surface rupture length]; Wells and Coppersmith, 1994).

CONCLUSION

We studied three sites showing horizontal (and vertical at places) offsets along the Ganzi fault, in the NW part of the Xianshuihe fault system in eastern Tibet, to evaluate its late Quaternary slip rate and assess the seismic hazard in this highly seismically active region. By measuring offset moraine crests and fan edges using LiDAR and kinematic GPS, and dating their surfaces using ^{10}Be (surface and depth profile) cosmogenic nuclides, we determined a constant late Quaternary (ca. 90–20 ka) slip rate along the Ganzi fault of 7 (+1.1/–1.0) mm/yr at the ZDG site, 3–11.2 mm/yr at the MGT/Ria sites, and 8.5 (+0.8/–0.7) mm/yr at the GZ site.

The ZDG site is the best constrained site, with precise offsets and tight ages. Its 6–8 mm/yr rate is compatible with our rate estimations at our two other sites, and we choose it to best represent the late Quaternary rate along the Ganzi fault. Furthermore, this rate is also compatible with geodetic (InSAR and GPS) and geologic (offsets of the Queer Range pluton and the Jinsha River, using low-temperature thermochronology) rate estimations. We conclude that the rate has remained constant along the entire Ganzi fault (~300 km) at all time scales since the fault initiation in the early Miocene (ca. 12.6 Ma). Such rates could potentially produce a devastating M 7.6 earthquake near Manigango. Initiation of the Xianshuihe fault system at ca. 12.6 Ma marked the onset of the present-day tectonic regime in SE Tibet and in Sundaland.

ACKNOWLEDGMENTS

This project was conducted under the auspices of the National Natural Science Foundation of China (NSFC 41672210, 41672211), the China Geological Survey (project DD20160022), the Basic Outlay of Scientific Research Work from the Institute of Geology, Chinese Academy of Geological Sciences (J1528), as well as the Cai Yuanpei program (27968UC) of the China Scholarship Council/French Ministry of Education. This work also benefited from help in the field from Haijian Lu, Shuai Han, Yuan Tang, and Kun Yun. We thank J. Van der Woerd from the University of Strasbourg/CNRS UMR7516 for the accelerator mass spectrometry measurements, which were performed at the ASTER (Accélérateur pour les Sciences de la Terre, Environnement, Risques) AMS (accelerator mass spectrometry) French national facility (CEREGE [Centre Européen de recherche et d'enseignement des

Géosciences de l'Environnement], Aix-en-Provence), supported by the INSU/CNRS (Institut National des Sciences de l'Univers/ Centre National de la Recherche Scientifique), the French Ministry of Research and Higher Education, IRD (Institut de recherche pour le developpement), and CEA (Commissariat à l'énergie atomique et aux énergies alternatives). We thank Claire Ansberque and an anonymous reviewer for their positive reviews and comments.

REFERENCES CITED

Allen, C.R., Luo, Z., Qian, H., Wen, X., Zhou, H., and Huang, W., 1991, Field study of a highly active fault zone: The Xianshuihe fault of southwestern China: Geological Society of America Bulletin, v. 103, p. 1178–1199, doi:10.1130/0016-7606(1991)103<1178:FSOAHA>2.3.CO;2.

Anderson, R.S., Repka, J.L., and Dick, G.S., 1996, Explicit treatment of inheritance in dating depositional surfaces using in situ ^{10}Be and ^{26}Al: Geology, v. 24, no. 1, p. 47–51, doi:10.1130/0091-7613(1996)024<0047:ETOIID>2.3.CO;2.

Applegate, P.J., Urban, N.M., Laabs, B.J.C., Keller, K., and Alley, R.B., 2010, Modeling the statistical distributions of cosmogenic exposure dates from moraines: Geoscientific Model Development, v. 3, p. 293–307, doi:10.1016/j.yqres.2011.12.002.

Balco, G., Stone, J.O., Lifton, N.A., and Dunai, T.J., 2008, A complete and easily accessible means of calculating surface exposure ages or erosion rates from ^{10}Be and ^{26}Al measurements: Quaternary Geochronology, v. 3, p. 174–195, doi:10.1016/j.quageo.2007.12.001.

Benedetti, L., and Van der Woerd, J., 2014, Cosmogenic nuclide dating of earthquakes, faults, and toppled blocks: Elements, v. 10, no. 5, p. 357–361, doi:10.2113/gselements.10.5.357.

Briner, J.P., Kaufman, D.S., Manley, W.F., and Finkel, R.C., 2005, Cosmogenic exposure dating of late Pleistocene moraine stabilization in Alaska: Geological Society of America Bulletin, v. 117, p. 1108–1120, doi:10.1130/B25649.1.

Cheng, J., Liu, J., Gan, W., Yu, H., and Li, G., 2011, Characteristics of strong earthquake evolution around the eastern boundary faults of the Sichuan-Yunnan rhombic block: Science China–Earth Sciences, v. 54, p. 1716–1729, doi:10.1007/s11430-011-4290-2.

Chevalier, M.-L., Hilley, G., Tapponnier, P., Van Der Woerd, J., Liu-Zeng, J., Finkel, R.C., Ryerson, F.J., Li, H., and Liu, X., 2011, Constraints on the late Quaternary glaciations in Tibet from cosmogenic exposure ages of moraine surfaces: Quaternary Science Reviews, v. 30, p. 528–554, doi:10.1016/j.quascirev.2010.11.005.

Chevalier, M.L., Leloup, P.H., Replumaz, A., Pan, J., Liu, D., Li, H., Gourbet, L., and Metois, M., 2016, Tectonic-geomorphology of the Litang fault system, SE Tibetan Plateau, and implication for regional seismic hazard: Tectonophysics, v. 682, p. 278–292, doi:10.1016/j.tecto.2016.05.039.

Clark, P.U., Dyke, A.S., Shakun, J.D., Carlson, A.E., Clark, J., Wohlfarth, B., Mitrovica, J.X., Hostetler, S.W., and McCabe, A.M., 2009, The Last Glacial Maximum: Science, v. 325, p. 710–714, doi:10.1126/science.1172873.

Cowgill, E., 2007, Impact of riser reconstructions on estimation of secular variation in rates of strike-slip faulting: Revisiting the Cherchen River site along the Altyn Tagh fault, NW China: Earth and Planetary Science Letters, v. 254, no. 3-4, p. 239–255, doi:10.1016/j.epsl.2006.09.015.

Desilets, D., Zreda, M., and Prabu, T., 2006, Extended scaling factors for in situ cosmogenic nuclides: New measurements at low latitude: Earth and Planetary Science Letters, v. 246, p. 265–276, doi:10.1016/j.epsl.2006.03.051.

Dunai, T.J., 2000, Scaling factors for production rates of in situ produced cosmogenic nuclides: a critical reevaluation: Earth and Planetary Science Letters, v. 176, p. 157–169, doi:10.1016/S0012821X(99)00310-6.

Dunai, T.J., 2001, Influence of secular variation of the geomagnetic field on the production rates of in situ produced cosmogenic nuclides: Earth and Planetary Science Letters, v. 193, p. 197–212 doi:10.1016/S0012-821X(01)00503-9.

Gan, W., Zhang, P., Shen, Z., Niu, Z., Wang, M., Wan, Y., Zhou, D., and Cheng, J., 2007, Present-day crustal motion within the Tibetan Plateau inferred from GPS measurements: Journal of Geophysical Research, v. 112, p. B08416, doi:10.1029/2005JB004120.

Gosse, J., and Phillips, F., 2001, Terrestrial in situ cosmogenic nuclides: Theory and application: Quaternary Science Reviews, v. 20, p. 1475–1560, doi:10.1016/S0277-3791(00)00171-2.

Hallet, B., and Putkonen, J., 1994, Surface dating of dynamic landforms: Young boulders on aging moraines: Science, v. 265, p. 937–940, doi:10.1126/science.265.5174.937.

Hancock, G.S., Anderson, R.S., Chadwick, O.A., and Finkel, R.C., 1999, Dating fluvial terraces with Be-10 and Al-26 profiles: Application to the Wind River, Wyoming: Geomorphology, v. 27, no. 1-2, p. 41–60, doi:10.1016/S0169-555X(98)00089-0.

Hanks, T.C., and Thatcher, W., 2006, The slip-rate discrepancy for the Altyn Tagh fault: An example of epistemic uncertainty: Eos (Washington, D.C.), v. 87, no. 52, Fall Meeting supplement, abstract T21E–03.

Hetzel, R., Niedermann, S., Tao, M.X., Kubik, P.W., Ivy-Ochs, S., Gao, B., and Strecker, M.R., 2002, Low slip rates and long-term preservation of geomorphic features in Central Asia: Nature, v. 417, p. 428–432, doi:10.1038/417428a.

Heyman, J., Stroeven, A.P., Harbor, J., and Caffee, M.W., 2011, Too young or too old: Evaluating cosmogenic exposure dating based on an analysis of compiled boulder exposure ages: Earth and Planetary Science Letters, v. 302, p. 71–80, doi:10.1016/j.epsl.2010.11.040.

Heyman, J., Applegate, P.J., Blomdin, R., Gribenski, N., Harbor, J.M., and Stroeven, A.P., 2016, Boulder height-exposure age relationships from a global glacial ^{10}Be compilation: Quaternary Geochronology, v. 34, p. 1–11, doi:10.1016/j.quageo.2016.03.002.

Hidy, A.J., Gosse, J.C., Pederson, J.L., Mattern, J.P., and Finkel, R.C., 2010, A geologically constrained Monte Carlo approach to modeling exposure ages from profiles of cosmogenic nuclides: An example from Lees Ferry, Arizona: Geochemistry Geophysics Geosystems, v. 11, p. Q0AA10, doi:10.1029/2010GC003084.

Huang, X., Du, Y., He, Z., Ma, B., and Xie, F., 2015a, Late Quaternary slip rate of the Batang fault and its strain partitioning role in Yushu area, Central Tibet: Tectonophysics, v. 653, p. 52–67, doi:10.1016/j.tecto.2015.03.026.

Huang, X., Du, Y., He, Z., Ma, B., and Xie, F., 2015b, Late Pleistocene–Holocene paleoseismology of the Batang fault (central Tibet Plateau, China): Geomorphology, v. 239, p. 127–141, doi:10.1016/j.geomorph.2015.03.026.

Imbrie, J., Hays, J.D., Martinson, D.G., McIntyre, A., Mix, A.C., Morley, J.J., Pisias, N.G., Prell, W.L., and Shackleton, N.J., 1984, The orbital theory of Pleistocene climate: Support from a revised chronology of the marine δ^{18}O record, *in* Berger, A., Imbrie, J., Hays, J., Kukla, G., and Saltzman, B., eds., Milankovitch and Climate: Understanding the Response to Astronomical Forcing: Boston, Reidel, p. 269–305.

Institute of Geophysics, China Earthquake Administration, Institute of Historic Geography, Fudan University (IGCEA and HGFU), 1990, The Atlas of Historic Earthquakes of China, Book for the Qing Dynasty: Beijing, China Cartographic Publishing House, 244 p. [in Chinese].

King, R.W., Shen, F., Burchfiel, B.C., Chen, Z., Li, Y., Liu, Y., Royden, L.H., Wang, E., Zhang, X., and Zhao, J., 1997, Geodetic measurement of crustal motion in southwest China: Geology, v. 25, p. 179–182, doi:10.1130/0091-7613(1997)025<0179:GMOCMI>2.3.CO;2.

Klinger, Y., 2010, Relation between continental strike-slip earthquake segmentation and thickness of the crust: Journal of Geophysical Research, v. 115, p. B07306, doi:10.1029/2009JB006550.

Lal, D., 1991, Cosmic-ray labeling of erosion surfaces—In situ nuclide production rates and erosion models: Earth and Planetary Science Letters, v. 104, no. 2-4, p. 424–439, doi:10.1016/0012-821X(91)90220-C.

Lehmkuhl, F., 1998, Extent and spatial distribution of Pleistocene glaciations in eastern Tibet: Quaternary International, v. 45–46, p. 123–134, doi:10.1016/S1040-6182(97)00010-4.

Leloup, P.H., Arnaud, N., Lacassin, R., Kienast, J.R., Harrison, T.M., Phan Trong, T.T., Replumaz, A., and Tapponnier, P., 2001, New constraints on the structure, thermochronology, and timing of the Ailao Shan–Red River shear zone, SE Asia: Journal of Geophysical Research, v. 106, p. 6683–6732, doi:10.1029/2000JB900322.

Li, C., Pang, J., and Zhang, Z., 2012, Characteristics, geometry, and segmentation of the surface rupture associated with the 14 April 2010 Yushu earthquake, eastern Tibet: China: Bulletin of the Seismological Society of America, v. 102, no. 4, p. 1618–1638, doi:10.1785/0120110261.

Li, Z., Elliott, J.R., Feng, W., Jackson, J.A., Parsons, B.E., and Walters, R.J., 2011, The 2010 MW 6.8 Yushu (Qinghai, China) earthquake: Constraints provided by InSAR and body wave seismology: Journal of Geophysical Research, v. 116, p. B10302, doi:10.1029/2011JB008358.

Liang, S., Gan, W., Shen, C., Xiao, G., Liu, J., Chen, W., Ding, X., and Zhou, D., 2013, Three- dimensional velocity field of present-day crustal motion of the Tibetan Plateau derived from GPS measurements: Journal of Geophysical Research, v. 118, no. 10, p. 5722–5732, doi:10.1002/2013JB010503.

Lifton, N., Bieber, J., Clem, J., Duldig, M., Evenson, P., Humble, J., and Pyle, R., 2005, Addressing solar modulation and long-term uncertainties in scaling secondary cosmic rays for in situ cosmogenic nuclide applications: Earth and Planetary Science Letters, v. 239, p. 140–161, doi:10.1016/j.epsl.2005.07.001.

Lin, A., Rao, G., Jia, D., Wu, X., Yan, B., and Ren, Z., 2011, Co-seismic strike-slip surface rupture and displacement produced by the 2010 MW 6.9 Yushu earthquake, China, and implications for Tibetan tectonics: Journal of Geodynamics, v. 52, p. 249–259, doi:10.1016/j.jog.2011.01.001.

Liu, Y., Xu, C., Li, Z., Wen, Y., and Forrest, D., 2011, Interseismic slip rate of the Garze–Yushu fault belt in the Tibetan Plateau from C-band InSAR observations between 2003 and 2010: Advances in Space Research, v. 48, p. 2005–2015, doi:10.1016/j.asr.2011.08.020.

Loveless, J.P., and Meade, B.J., 2011, Partitioning of localized and diffuse deformation in the Tibetan Plateau from joint inversions of geologic and geodetic observations: Earth and Planetary Science Letters, v. 303, p. 11–24, doi:10.1016/j.epsl.2010.12.014.

Matmon, A., Simhai, O., Amit, R., Haviv, I., Porat, N., McDonald, E., Benedetti, L., and Finkel, R.C., 2009, Desert pavement–coated surfaces in extreme deserts present the longest-lived landforms on Earth: Geological Society of America Bulletin, v. 121, no. 5/6, p. 688–697, doi:10.1130/B26422.1.

Meade, B.J., 2007, Present-day kinematics at the India-Asia collision zone: Geology, v. 35, no. 1, p. 81–84, doi:10.1130/G22924A.1.

Molnar, P., and Deng, Q., 1984, Faulting associated with large earthquakes and the average rate of deformation in central and eastern Asia: Journal of Geophysical Research, v. 89, p. 6203–6227, doi:10.1029/JB089iB07p06203.

Ou, X., Lai, Z., Zhou, S., and Zeng, L., 2014, Timing of glacier fluctuations and trigger mechanisms in eastern Qinghai–Tibetan Plateau during the late Quaternary: Quaternary Research, v. 81, p. 464–475, doi:10.1016/j.yqres.2013.09.007.

Papadimitriou, E., Wen, X., Karakostas, V., and Jin, X., 2004, Earthquake triggering along the Xianshuihe fault zone of western Sichuan, China: Pure and Applied Geophysics, v. 161, p. 1683–1707, doi:10.1007/s00024-003-2471-4.

Perfettini, H., and Avouac, J.P., 2004, Postseismic relaxation driven by brittle creep: A possible mechanism to reconcile geodetic measurements and the decay rate of aftershocks, application to the Chi-Chi earthquake, Taiwan: Journal of Geophysical Research, v. 109, p. B02304, doi:10.1029 /2003JB002488.

Putkonen, J., and Swanson, T., 2003, Accuracy of cosmogenic ages for moraines: Quaternary Research, v. 59, p. 255–261, doi:10.1016/S0033-5894(03)00006-1.

Reid, A., Wilson, C.J., Shun, L., Pearson, N., and Belousova, E., 2007, Mesozoic plutons of the Yidun arc, SW China: U/Pb geochronology and Hf isotopic signature: Ore Geology Reviews, v. 31, no. 1, p. 88–106, doi:10.1016/j.oregeorev.2004.11.003.

Repka, J.L., Anderson, R.S., and Finkel, R.C., 1997, Cosmogenic dating of fluvial terraces, Fremont River, Utah: Earth and Planetary Science Letters, v. 152, p. 59–73, doi:10.1016/S0012-821X(97)00149-0.

Roger, F., Calassou, S., Lancelot, J., Malavieille, J., Mattauer, M., Xu, Z., Hao, Z., and Hou, L., 1995, Miocene emplacement and deformation of the Konga Shan granite (Xianshui He fault zone, west Sichuan, China): Geodynamic implications: Earth and Planetary Science Letters, v. 130, p. 201–216, doi:10.1016/0012-821X(94)00252-T.

Rogers, G., and Dragert, H., 2003, Episodic tremor and slip on the Cascadia subduction zone: The chatter of silent slip: Science, v. 300, p. 1942, doi:10.1126/science.1084783.

Roth, F., 1989, A model for the present stress field along the Xian-shui-he fault belt, northwest Sichuan, China, *in* Berry, M.J., ed., Earthquake Hazard Assessment and Prediction: Tectonophysics, v. 167, p. 103–115, doi:10.1016/0040-1951(89)90061-9.

Savage, J.C., and Prescott, W.H., 1978, Asthenosphere readjustment and the earthquake cycle: Journal of Geophysical Research, v. 83, p. 3369–3376, doi:10.1029 / JB083iB07p03369 .

Segall, P., 2002, Integrating geologic and geodetic estimates of slip rate on the San Andreas fault system: International Geology Review, v. 44, p. 62–82, doi:10.2747/0020-6814.44.1.62.

Shen, Z., Lu, J., Wang, M., and Burgmann, R., 2005, Contemporary crustal deformation around the southeast borderland of the Tibetan Plateau: Journal of Geophysical Research, v. 110, p. B11409, doi:10.1029/2004JB003421.

Shi, F., He, H., Densmore, A.L., Li, A., Yang, X., and Xu, X., 2016, Active tectonics of the Ganzi-Yushu fault in the southeastern Tibetan Plateau: Tectonophysics, v. 676, p. 112–124, doi:10.1016/j.tecto.2016.03.036.

Stone, J.O., 2000, Air pressure and cosmogenic isotope production: Journal of Geophysical Research, v. 105, p. 23,753–23,759, doi:10.1029/2000JB900181.

Strasky, S., Graf, A.A., Zhao, Z.Z., Kubik, P.W., Baur, H., Schluchter, C., and Wieler, R., 2009, Late Glacial ice advances in southeast Tibet: Journal of Asian Earth Sciences, v. 34, p. 458–465, doi:10.1016/j.jseaes.2008.07.008.

Tapponnier, P., and Molnar, P., 1976, Slip-line field theory and large-scale continental tectonics: Nature, v. 264, no. 5584, p. 319–324, doi:10.1038/264319a0.

Thatcher, W., 2007, Microplate model for the present-day deformation of Tibet: Journal of Geophysical Research, v. 112, p. B01401, doi:10.1029/2005JB004244.

Thompson, L.G., Yao, T., Davis, M.E., Henderson, K.A., Mosley-Thompson, E., Lin, P.N., Beer, J., Synal, H.-A., Cole-Dai, J., and Bolzan, J.F., 1997, Tropical climate instability: The last glacial cycle from a Qinghai-Tibetan ice core: Science, v. 276, p. 1821–1825, doi:10.1126/science.276.5320.1821.

Tobita, M., Nishimura, T., Kobayashi, T., Hao, K.X., and Shindo, Y., 2011, Estimation of coseismic deformation and a fault model of the 2010 Yushu earthquake using PALSAR interferometry data: Earth and Planetary Science Letters, v. 307, p. 430–438, doi:10.1016/j.epsl.2011.05.017.

Wang, E., and Burchfiel, B.C., 2000, Late Cenozoic to Holocene deformation in southwestern Sichuan and adjacent Yunnan, China, and its role in formation of the southeastern part of the Tibetan Plateau: Geological Society of America Bulletin, v. 112, p. 413–423, doi:10.1130/0016-7606(2000)112<413:LCTHDI>2.0.CO;2.

Wang, E., Burchfiel, B.C., Royden, L.H., Chen, L., Chen, J., Li, W., and Chen, Z., 1998, The Cenozoic Xianshuihe–Xiaojiang, Red River, and Dali Fault Systems of Southwestern Sichuan and Central Yunnan, China: Geological Society of America Special Paper 327, 108 p., doi:10.1130/0-8137-2327-2.1.

Wang, S., Fang, X., Zheng, D., and Wang, E., 2009, Initiation of slip along the Xianshuihe fault zone, eastern Tibet, constrained by K/Ar and fission-track ages: International Geology Review, v. 51, no. 12, p. 1121–1131, doi:10.1080/00206810902945132.

Wang, W., Qiao, X., Yang, S., and Wang, D., 2017, Present-day velocity field and block kinematics of Tibetan Plateau from GPS measurements: Geophysical Journal International, v. 208, no. 2, p. 1088–1102, doi:10.1093/gji/ggw445.

Wang, Y., Wang, E., Shen, Z., Wang, M., Gan, W., Qiao, X., Meng, G., Li, T., Tao, W., and Yang, Y., 2008, GPS-constrained inversion of present-day slip rates along major faults of the Sichuan–Yunnan region: China Science, ser. D, v. 51, no. 9, p. 1267–1283, doi:10.1007/s11430-008-0106-4.

Wang, Y., Wang, M., Shen, Z., Ge, W., Wang, K., Wang, F., and Sun, J., 2013, Inter-seismic deformation field of the Ganzi-Yushu fault before the 2010 Mw 6.9 Yushu earthquake: Tectonophysics, v. 584, p. 138–143, doi:10.1016/j.tecto.2012.03.026.

Wells, D.L., and Coppersmith, K.J., 1994, New empirical relationships among magnitude, rupture length, rupture width, rupture area, and surface displacement: Bulletin of the Seismological Society of America, v. 84, p. 974–1002.

Wen, X., 2000, Character of rupture segment of Xianshuihe-Zemuhe–Anninghe fault zone, western Sichuan: Seismology and Geology, v. 22, p. 239–249.

Wen, X., Xu, X., Zheng, R., Xie, Y., and Wan, C., 2003, Average slip-rate and recent large earthquake ruptures along the Ganzi-Yushu fault: Science in China, v. 46, p. 276–288.

Wen, X.Z., Ma, S.L., Xu, X.W., and He, Y.N., 2008, Historical pattern and behavior of earthquake ruptures along the eastern boundary of the Sichuan–Yunnan faulted-block, southwestern China: Physics of the Earth and Planetary Interiors, v. 168, no. 1-2, p. 16–36, doi:10.1016/j.pepi.2008.04.013.

Xu, L.B., and Zhou, S.Z., 2009, Quaternary glaciations recorded by glacial and fluvial landforms in the Shaluli Mountains, southeastern Tibetan Plateau: Geomorphology, v. 103, p. 268–275, doi:10.1016/j.geomorph.2008.04.015.

Xu, L.B., Ou, X.J., Lai, Z.P., Zhou, S.Z., Wang, J., and Fu, Y.C., 2010, Timing and style of late Pleistocene glaciation in the Queer Shan, northern Hengduan Mountains, in the eastern Tibetan Plateau: Journal of Quaternary Science, v. 25, p. 957–966, doi:10.1002/jqs.1379.

Xu, X., Wen, X., Zheng, R., Ma, W., Song, F., and Yu, G., 2003, Pattern of latest tectonic motion and its dynamics for active blocks in Sichuan-Yunnan region, China: Science in China, v. 46, p. 210–226, doi:10.1360/03dz0017.

Yan, B., and Lin, A., 2015, Systematic deflection and offset of the Yangtze River drainage system along the strike-slip Ganzi-Yushu-Xianshuihe fault zone, Tibetan Plateau: Journal of Geodynamics, v. 87, p. 13–25, doi:10.1016/j.jog.2015.03.002.

Zechar, J.D., and Frankel, K.L., 2009, Incorporating and reporting uncertainties in fault slip rates: Journal of Geophysical Research, v. 114, p. B12407, doi:10.1029/2009JB006325.

Zhang, B., Ou, X.J., and Lai, Z.P., 2012, OSL ages revealing the glacier retreat in the Dangzi valley in the eastern Tibetan Plateau during the Last Glacial Maximum: Quaternary Geochronology, v. 10, p. 244–249, doi:10.1016/j.quageo.2012.01.013.

Zhang, G., Shan, X., and Feng, G., 2016, The 3-D surface deformation, coseismic fault slip and after-slip of the 2010 Mw6.9 Yushu earthquake, Tibet, China: Journal of Asian Earth Sciences, v. 124, p. 260–268, doi:10.1016/j.jseaes.2016.05.011.

Zhang, P., Sheng, Z., Wang, M., Gan, W., Burgmann, R., Molnar, P., Wang, Q., Niu, Z., Sun, J., Wu, J., Sun, H., and You, X., 2004, Continuous deformation of the Tibetan Plateau from global positioning system data: Geology, v. 32, p. 809–812, doi:10.1130/G20554.1.

Zhang, P.Z., 2013, A review on active tectonics and deep crustal processes of the western Sichuan region, eastern margin of the Tibetan Plateau: Tectonophysics, v. 584, p. 7–22, doi:10.1016/j.tecto.2012.02.021.

Zhang, Y., Replumaz, A., Wang, G., Leloup, P.H., Gautheron, C., Bernet, M., Van der Beek, P., Paquette, J.L., Wang, A., Zhang, K., Chevalier, M.L., and Li, H., 2015, Timing and rate of exhumation along the Litang fault system, implication for fault reorganization in southeast Tibet: Tectonics, v. 34, p. 1219–1243, doi:10.1002/2014TC003671.

Zhang, Y., Yao, X., Yu, K., Du, G., and Guo, C., 2016, Late Quaternary slip-rate and seismic activity of the Xianshuihe fault zone in southwest China: Acta Geologica Sinica, v. 90, p. 525–536, doi:10.1111/1755-6724.12688.

Zhang, Y., Replumaz, A., Leloup, P.H., Wang, G., Bernet, M., van der Beek, P., Paquette, J.L., Chevalier, M.L., 2017, Cooling history of the Gongga batholith: Implications for the Xianshuihe Fault and Miocene kinematics of SE Tibet: Earth and Planetary Science Letters, v. 465, p. 1–15, doi:10.1016/j.epsl.2017.02.025.

Zhao, B., Huang, Y., Zhang, C., Wang, W., Tan, K., and Du, R., 2015, Crustal deformation on the Chinese mainland during 1998–2014 based on GPS data: Geodesy and Geodynamics, v. 6, p. 7–15, doi:10.1016/j.geog.2014.12.006.

Zhou, H., Liu, H., and Kanamori, H., 1983, Source processes of large earthquakes along the Xianshuihe fault in southwestern China: Bulletin of the Seismological Society of America, v. 73, p. 537–551.

Zhou, R., Ma, S., and Cai, C., 1996, Late Quaternary active features of the Ganzi–Yushu fault zone: Earthquake Research in China, v. 12, no. 3, p. 250–260 [in Chinese].

Zhou, R., Wen, X., Cai, C., and Ma, S., 1997, Recent earthquakes and assessment of seismic tendency on the Ganzi–Yushu fault zone: Seismology and Geology, v. 19, no. 2, p. 115–124 [in Chinese].

Zhou, R., Li, Y., Liang, M., Xu, X., He, Y., Wang, S., Ma, C., and Liu, Y., 2014, Determination of mean recurrence interval of large earthquakes on the Garze-Yushu fault (Dengke segment) on the eastern margin of the Qinghai-Tibetan Plateau: Quaternary International, v. 333, p. 179–187, doi:10.1016/j.quaint.2013.11.010.

Zielke, O., Klinger, Y., and Arrowsmith, J., 2015, Fault slip and earthquake recurrence along strike-slip faults—Contributions of high-resolution geomorphic data: Tectonophysics, v. 638, p. 43–62, doi:10.1016/j.tecto.2014.11.004.

Science Editor: David I. Schofield
Associate Editor: Xixi Zhao

Manuscript Received 27 October 2016
Revised Manuscript Received 26 April 2017
Manuscript Accepted 14 June 2017

Printed in the USA